

University of Alberta

**Structure, Superfluidity and Quantum
Melting of Hydrogen Clusters: A
Quantum Monte Carlo Study**

by

Fabio Mezzacapo



A thesis submitted to the Faculty of Graduate Studies and Research in partial fulfillment of the requirements for the degree of Doctor of Philosophy

Department of Physics

Edmonton, Alberta
Spring 2008



Library and
Archives Canada

Bibliothèque et
Archives Canada

Published Heritage
Branch

Direction du
Patrimoine de l'édition

395 Wellington Street
Ottawa ON K1A 0N4
Canada

395, rue Wellington
Ottawa ON K1A 0N4
Canada

Your file Votre référence
ISBN: 978-0-494-45567-8
Our file Notre référence
ISBN: 978-0-494-45567-8

NOTICE:

The author has granted a non-exclusive license allowing Library and Archives Canada to reproduce, publish, archive, preserve, conserve, communicate to the public by telecommunication or on the Internet, loan, distribute and sell theses worldwide, for commercial or non-commercial purposes, in microform, paper, electronic and/or any other formats.

The author retains copyright ownership and moral rights in this thesis. Neither the thesis nor substantial extracts from it may be printed or otherwise reproduced without the author's permission.

AVIS:

L'auteur a accordé une licence non exclusive permettant à la Bibliothèque et Archives Canada de reproduire, publier, archiver, sauvegarder, conserver, transmettre au public par télécommunication ou par l'Internet, prêter, distribuer et vendre des thèses partout dans le monde, à des fins commerciales ou autres, sur support microforme, papier, électronique et/ou autres formats.

L'auteur conserve la propriété du droit d'auteur et des droits moraux qui protègent cette thèse. Ni la thèse ni des extraits substantiels de celle-ci ne doivent être imprimés ou autrement reproduits sans son autorisation.

In compliance with the Canadian Privacy Act some supporting forms may have been removed from this thesis.

Conformément à la loi canadienne sur la protection de la vie privée, quelques formulaires secondaires ont été enlevés de cette thèse.

While these forms may be included in the document page count, their removal does not represent any loss of content from the thesis.

Bien que ces formulaires aient inclus dans la pagination, il n'y aura aucun contenu manquant.

■*■
Canada

ABSTRACT

The properties of pristine and isotopically doped clusters of molecular hydrogen (both *para*-hydrogen and *ortho*-deuterium) at low temperature (down to 0.0625 K) are studied theoretically, by means of computer simulations based on the Continuous-space Worm Algorithm. Different model interactions have been used; the basic physical conclusions are independent of the intermolecular potential, which only causes a shift in the temperature scale. The superfluid response at low temperature displays strong variation with the number N of molecules in the cluster, reflecting structural changes that occur by adding or removing even a single molecule. Clusters of specific sizes display *quantum melting*, going from solid-like to liquid-like as the temperature is lowered. This intriguing behavior is caused by quantum exchanges of molecules. Superfluid response of pure *para*-hydrogen clusters dramatically decreases when few molecules are substituted by *ortho*-deuterium ones. This finding suggests that superfluidity correlates with long exchanges of identical molecules in the entire cluster. Estimates of the local superfluid density confirm such a suggestion, showing that significant superfluid response is only seen when both the inner and the outer part of the system are superfluid and liquid-like, as a result of the occurrence of long permutational cycles involving all molecules.

ACKNOWLEDGMENTS

I wish to thank all the people who have supported me in several different ways during my PhD program. First of all Massimo Boninsegni, who has directed my research effort being for me an unlimited source of good advice, as well as an example from the professional and human point of view. Without his guidance and patient dedication, little or none of this work would have been possible. I am also extremely grateful to Antonella, for her precious and constant help with everyday problems, and for making me feel at home during the holidays (and not only) I have spent here in Edmonton.

I can not forget my office mates Joe and Long and the little chats we had between one “qsub” and one “ssh”. Their presence has been fundamental to make my working days more effective and pleasant. I would like to thank Daniel, Aditya, Giang, Neda, Amsalu and all the other fellows in room 213, for the friendly atmosphere they have been able to create and maintain in the office. I am also grateful to Javier for the useful discussions we had on the subject of this thesis.

A very special thanks goes to Mehmet for several dinners at his place and much, much more.

Finally I want to thank my family (all included!!!) and all my lifelong friends (non ho spazio per declinare le generalita'... e forse e' pure meglio!!!).

Words are not enough to thank Chiara.

This work was supported in part by the Natural Science and Engineering Research Council of Canada, under research grant 121210893, and by the Informatics Circle of Research Excellence (iCORE). Computer simulations were performed on the Mammouth cluster at University of Sherbrooke (Québec, Canada).

Table of Contents

INTRODUCTION	1
1 PHYSICAL MODEL AND METHODOLOGY	12
1.1 Many-body Hamiltonian	12
1.2 Computational methods	14
1.3 Potentials	15
1.4 Path Integrals	19
1.4.1 Quantum statistics	22
1.4.2 Numerical implementation	22
1.5 Metropolis algorithm	25
1.6 Continuous-space Worm Algorithm	27
1.6.1 Metropolis updates	29
1.7 Details of the simulation	36
1.7.1 High-temperature density matrix	36
1.7.2 Thermodynamic estimators	37
1.7.3 Evaluation of the statistical errors	39
2 RESULTS	42
2.1 p -H ₂ clusters	42
2.1.1 Energetics	42
2.1.2 Superfluidity	46
2.1.3 Quantum melting	53
2.2 o -D ₂ clusters	58
2.2.1 Energetics	59
2.2.2 Superfluidity	60
2.2.3 Structure	64
2.3 Isotopically doped p -H ₂ clusters	67
2.4 50/50 Mixed clusters	75
2.5 Local superfluidity of p -H ₂ clusters	77
2.6 Dependence of the numerical estimates on the interaction potential	85

TABLE OF CONTENTS

CONCLUSIONS	89
Bibliography	94

List of Figures

1	Schematic diagram of a HENDI spectroscopy experimental apparatus. [Reprinted with permission from Ref. [21]].	4
2	Infrared spectra of an OCS molecule embedded in a cluster of ^4He (a) and ^3He (b) atoms. Evolution of the spectrum in b when an increasing number of ^4He atoms is added (c-f). Temperature is 0.38 K. [Reprinted with permission from Ref. [21]].	5
1.1	Functional form of the Buck, LJ and SG potential.	18
1.2	Schematic representation of the paths of two particles in imaginary time. In this example, $M=5$, and the two particles undergo an exchange.	24
1.3	Schematic representation of one configuration in the G -sector, for a system of five particles in one dimension. This configuration contains four closed and one open world line, namely the worm, whose head (I) and tail (M) are indicated in picture.	28
1.4	Configuration of three particles before (left) and after (right) a swap update.	32
2.1	Energy per $p\text{-H}_2$ molecule versus cluster size N , at $T=1$ K. Estimates have been obtained using the SG (circles) and the Buck (boxes) potential. When not shown, statistical errors are of the order of, or smaller than the symbol size. Solid line is only a guide to the eye. Also shown for comparison are results from Ref. [35] (triangles). . .	43
2.2	Chemical potential of $p\text{-H}_2$ clusters versus cluster size N . Estimates have been obtained using the SG potential. When not shown, statistical errors are of the order of, or smaller than the symbol size. Solid line is only a guide to the eye. Numbers refer to stable ("magic") clusters.	45

LIST OF FIGURES

2.3	Temperature dependence of the superfluid fraction $\rho_S(T)$ for a cluster of 18 $p\text{-H}_2$ molecules (circles). Estimates are obtained with the SG potential. Dotted line is only a guide to the eye. When not shown, statistical errors are smaller than the symbol size. Also shown for comparison are results from Ref. [35] (triangles).	47
2.4	Superfluid fraction of $p\text{-H}_2$ clusters versus cluster size N , at $T=1$ K. Estimates have been obtained using the SG (circles) and the Buck (boxes) potential. When not shown, statistical errors are of the order of, or smaller than the symbol size. Solid line is only a guide to the eye. Also shown for comparison are results from Ref. [35] (triangles).	48
2.5	Radial density, at $T=1$ K, computed with respect to the center of mass, for clusters with 15, 25, 26, and 27 $p\text{-H}_2$ molecules. Estimates have been obtained using the SG potential. Statistical errors, not shown for clarity, are of the order of $5 \times 10^{-4} \text{ \AA}^{-3}$ or less.	50
2.6	Three dimensional representation of a cluster comprising 25 and 26 $p\text{-H}_2$ molecules (interacting via the SG potential) at a temperature of 1 K. Even though the information provided by this kind of figure is purely qualitative, the structural difference is evident: $(p\text{-H}_2)_{25}$ is essentially liquid-like (molecules are highly delocalized), while $(p\text{-H}_2)_{26}$ is solid-like (molecules are more localized and clearly distinguishable).	51
2.7	Statistics of permutation cycles involving $1 \leq M \leq N$ molecules for the clusters $(p\text{-H}_2)_{13}$ (a), $(p\text{-H}_2)_{18}$ (b), $(p\text{-H}_2)_{26}$ (c) and $(p\text{-H}_2)_{33}$ (d) at $T=1$ K. SG potential has been used.	52
2.8	Potential energy per molecule and superfluid fraction observed during a typical Monte Carlo run (see text) for a cluster of $N=23$ $p\text{-H}_2$ molecules at $T=1$ K (panels a and b) and $T=1.4$ K (panels c and d). Estimates have been obtained using the SG potential. The coexistence of two phases can be easily recognized since the averages of ρ_S and V simultaneously switch between high (liquid-like superfluid phase) and low (solid-like insulating phase) values. The liquid-like superfluid phase becomes dominant as T is lowered.	54
2.9	Potential energy per molecule and superfluid fraction recorded during a typical Monte Carlo run for a cluster of $N=18$ $p\text{-H}_2$ molecules at $T=2$ K. Estimates are obtained with the SG potential. In this case, ρ_S and V simply oscillate around their average values (approximately 0.6 for ρ_S) without featuring the clear, simultaneous "jumps" observed in Fig 2.8. This system is found to be liquid-like in the range of temperature considered in this work.	56

LIST OF FIGURES

2.10	Radial density profiles for a p -H ₂ cluster with $N=18$ [$T=0.75$ K (boxes) and $T=2$ K (triangles)] and $N=23$ [$T=0.75$ K (diamonds) and $T=2$ K (stars)] p -H ₂ molecules. Estimates have been obtained with the SG potential. Statistical errors, not shown for clarity, are of the order of $5 \times 10^{-4} \text{ \AA}^{-3}$ or less.	57
2.11	Energy per o -D ₂ molecules e versus cluster size N at a temperature of 0.5 K. Statistical errors are smaller than the symbol size. Solid line is only a guide to the eye.	59
2.12	Chemical potential of o -D ₂ clusters versus cluster size N . When not shown, statistical errors are of the order of, or smaller than the symbol size. Solid line is only a guide to the eye. Numbers refer to stable ("magic") clusters.	60
2.13	Temperature dependence of the superfluid fraction $\rho_S(T)$ for a clusters of 11 o -D ₂ molecules. Dotted line is only a guide to the eye. When not shown, statistical errors are smaller than the symbol size.	61
2.14	Statistics of permutation cycles involving $1 \leq M \leq N$ molecules for the cluster $(o\text{-D}_2)_{11}$ at $T=0.5$ K (lower panel) and $T=2$ K (upper panel).	62
2.15	Superfluid fraction of o -D ₂ clusters versus cluster size N , at $T=0.5$ K (circles) and $T=2$ K (boxes). When not shown, statistical errors are of the order of, or smaller than the symbol size. Solid lines are only guides to the eye.	63
2.16	Radial density profiles for o -D ₂ clusters with $N=7, 10$ and 11 , at $T=0.5$ K. The inset shows the radial density profiles of $(o\text{-D}_2)_{13}$ and $(p\text{-H}_2)_{13}$ at the same temperature. Statistical errors, omitted for clarity, are of the order of $5 \times 10^{-4} \text{ \AA}^{-3}$ or less.	65
2.17	Three-dimensional representation of clusters comprising 18 and 19 o -D ₂ molecules, at $T=0.5$ K. Both systems have solid-like properties, as molecules enjoy a high degree of localization. However, $(o\text{-D}_2)_{19}$ features greater stability, due to its more symmetric structure (see text).	66
2.18	Superfluid fraction ρ_{SH} of the <i>para</i> -hydrogen component in clusters of N molecules with one (circles), two (triangles) and four (squares) substitutional <i>ortho</i> -deuterium molecules, and with one (stars) <i>ortho</i> -hydrogen molecule. Upper panel shows data at $T=0.5$ K, lower at $T=1$ K. Open diamonds show results for the undoped clusters (entirely superfluid at $T=0.5$ K). Error bars are comparable to the size of the symbols.	68

LIST OF FIGURES

2.19	Radial density profiles for a pure $(p\text{-H}_2)_{25}$ (lower peak at short r) and a $(p\text{-H}_2)_{24}\text{-}(o\text{-D}_2)_1$ cluster, at $T=1$ K. Profiles are computed with respect to the geometrical center of the cluster. In the case of the doped cluster, no distinction is made between molecules of different types. Statistical errors are not shown for clarity; they are of the order of $5.0 \times 10^{-4} \text{ \AA}^{-3}$	69
2.20	Radial density profiles of the two components of the cluster $(p\text{-H}_2)_{24}\text{-}(o\text{-D}_2)_1$ (at a temperature of 1 K) taken separately. Profiles are computed with respect to the geometrical center of the cluster.	70
2.21	Radial density (multiplied by r^2) for the single $o\text{-D}_2$ and $o\text{-H}_2$ impurities in the doped $(p\text{-H}_2)_{24}\text{-}(o\text{-D}_2)_1$ and $(p\text{-H}_2)_{24}\text{-}(o\text{-H}_2)_1$ clusters, at a temperature of 1 K. Profiles are computed with respect to the geometrical center of the cluster.	71
2.22	Three-dimensional representations of the clusters $(p\text{-H}_2)_{16}\text{-}(o\text{-D}_2)_4$ (A) and of $(p\text{-H}_2)_{20}$ (B). Darker color is used for impurity molecules.	72
2.23	Frequency of occurrence of exchange cycles of length M (i.e., involving $1 \leq M \leq N_H$ $p\text{-H}_2$ molecules) at $T=1$ K. Spikes from left to right refer to a pristine $(p\text{-H}_2)_{25}$ cluster and to the mixtures $(p\text{-H}_2)_{24}\text{-}(o\text{-H}_2)_1$ and $(p\text{-H}_2)_{24}\text{-}(o\text{-D}_2)_1$	74
2.24	Number of $p\text{-H}_2$ (circles) and $o\text{-D}_2$ (triangles) molecules in the superfluid phase in mixed clusters of varying size N and equal concentration of the two isotopes (i.e., $N_H = N_D = N/2$) at $T=0.5$ K.	75
2.25	Three dimensional representation of the cluster $(p\text{-H}_2)_5\text{-}(o\text{-D}_2)_5$ (A) and $(p\text{-H}_2)_{10}\text{-}(o\text{-D}_2)_{10}$ (B) at a temperature of 0.5 K; $o\text{-D}_2$ molecules are rendered in darker color.	76
2.26	Profiles of total $[n(r)]$ and superfluid $[n_S(r)]$ density computed with respect to the center of mass of the cluster $(p\text{-H}_2)_{18}$ at $T=1$ K (lower panel), $T=2$ K (middle panel) and $T=3$ K (upper panel).	79
2.27	Profiles of total and superfluid density at $T=0.0625$ K (solid line and circles), $T=0.25$ K (dashed line and triangles) and $T=0.5$ K (dotted line and diamonds) for the cluster $(p\text{-H}_2)_{26}$	80
2.28	Frequency of occurrence of permutation cycles involving M molecules in a cluster of 26 $p\text{-H}_2$ molecules at $T=0.5$ K (lower values) and $T=0.0625$ K (higher values). Long permutation cycles set in at low T	82
2.29	Profiles of total and superfluid density for the cluster $(p\text{-H}_2)_{25}$ (solid line and circles), $(p\text{-H}_2)_{26}$ (dotted line and diamonds), $(p\text{-H}_2)_{27}$ (dashed line and triangles) at $T=0.5$ K. Open symbols show estimates of the local superfluid density obtained for the cluster $(p\text{-H}_2)_{25}$ using the same measure utilized in Ref. [42].	83

LIST OF FIGURES

2.30	Energy per p -H ₂ molecule as a function of the cluster size N at $T=1$ K. Estimates are obtained using the Buck (diamonds), SG (circles) and LJ (triangles) potential.	85
2.31	Superfluid fraction of p -H ₂ clusters versus cluster size N at $T=1$ K (filled symbols) and $T=0.5$ K (open symbols). Estimates have been obtained using the SG (circles), Buck (diamonds) and LJ (triangles) potential.	87
2.32	Potential energy per molecule and superfluid fraction observed during a typical Monte Carlo run for a cluster of $N=26$ p -H ₂ molecules at $T=1$ K (panels a and b) and $T=1.5$ K (panels c and d). The coexistence of two phases can be easily recognized since the averages of ρ_S and V simultaneously switch between high (liquid-like superfluid phase) and low (solid-like insulating phase) values. The liquid-like superfluid phase becomes dominant as T is lowered. Results are obtained with the LJ potential.	88
2.33	Radial density profiles for a p -H ₂ cluster with $N=26$ at $T=0.0625$ K (solid line) and $T=1$ K (dashed line). The system undergoes quantum melting at low T . Statistical errors, not shown for clarity, are of the order of $5 \times 10^{-4} \text{ \AA}^{-3}$ or less, results are obtained with the Buck potential.	89

INTRODUCTION

The superfluid phase of matter can be observed in the liquid phase of both isotopes of helium, below a critical temperature $T = T_\lambda = 2.177$ K for ^4He and approximately 2 mK for ^3He [1]. The term “superfluidity” (SF) was coined by Kapitsa [2], to indicate the ability of liquid ^4He to flow (at $T < T_\lambda$) with no measurable viscosity through a microscopic gap between two disks¹. In order to explain the apparent contradiction between these findings, and the finite viscosity measured by Keesom and MacWood by means of an oscillating disk dipped in a helium bath [4], Tisza proposed a *two-fluid model* [5], according to which below T_λ liquid helium consists of two distinct components: one is *normal* (viscous), the other *superfluid* (non-viscous), the latter becoming dominant in bulk liquid helium as T approaches 0 K. Such a phenomenological picture accounts quantitatively for the experimental result of Andronikashvili, who observed the progressive decrease of the moment of inertia of a torsional oscillator in helium, as T decreases below T_λ . This is interpreted as the sign of the increase of the helium superfluid component, which is decoupled from the oscillator rotation [6].

In the last 70 years, SF has been the subject of intense experimental and theoretical investigation. Its connection to *superconductivity*, another phenomenon

¹The same experimental observation was made independently by Allen and Misener [3].

which manifests itself in the form of dissipation-less flow, one with potential important technological applications, renders the microscopic understanding of SF one of the most important problems in condensed matter and many-body physics. A particularly intriguing question is whether it is possible to detect SF in condensed phases of atomic or molecular species other than helium. Indeed, observing the same phenomenon in different physical systems is often the key to gaining further understanding. Enormous technical advances made over the past decade in the experimental trapping and laser cooling of cold atoms, have allowed the observation of SF in a highly controlled, artificial setting [7]. Still, the search for a second, *naturally occurring* superfluid is widely regarded as a worthwhile goal.

Fluids made of light bosonic molecules such as *para*-hydrogen ($p\text{-H}_2$) or *ortho*-deuterium ($o\text{-D}_2$), whose mass is smaller than (or equal to) that of helium atoms, have long been regarded as potential superfluids. Indeed, it was first noted by Ginzburg and Sobyenin [8], that the same simple argument based on a non-interacting Bose gas, predicting a Bose-Einstein Condensation transition (believed to coincide with the superfluid one [1]) for ^4He at approximately 3.3 K (i.e., surprisingly close to the experimental T_λ), would predict a transition for a $p\text{-H}_2$ fluid at approximately 6.5 K, on account of the lighter molecular mass. However, there is a fundamental physical difference between condensed helium and hydrogen; unlike helium, which under its own vapor pressure remains a liquid all the way down to zero temperature, owing to the weakness of the interaction between two helium atoms, the considerably stronger attractive interaction between two hydrogen molecules results in an equilibrium crystal phase, with a freezing temperature of 13.8 K, significantly higher than that at which a superfluid transition might take place [9]. Several attempts have been made [10, 11, 12, 13] to supercool bulk liquid

p -H₂, but the search for SF (in the bulk) has so far not met with success.

Confinement, and reduction of dimensionality, are deemed plausible avenues to stabilize a metastable liquid phase down to temperatures sufficiently low that a superfluid transition may be observed. However, theoretical studies of p -H₂ films adsorbed on various substrates [14, 15, 16], as well as in two mathematical dimensions [17], have so far yielded no hint of possible SF. The suggestion was made that SF may occur in a strictly two-dimensional (2D) p -H₂ fluid embedded in a crystalline matrix of Alkali atoms [18]. That prediction was actually based on numerical simulations of model systems of very small size, and was subsequently disproven by more accurate calculations, showing that the superfluid signal observed in Ref. [18] was merely an artifact of the very small system size utilized [19].

On the other hand, sufficiently small clusters of p -H₂ molecules may remain “liquid-like” at significantly lower T than the bulk, and therefore SF could occur at temperatures which could conceivably render its observation possible. Indeed, a recently introduced experimental technique, known as Helium NanoDroplet Isolation spectroscopy (HENDI), allows one to investigate a single molecular impurity embedded in clusters comprising from a few, to several thousand He atoms [20]. In these experiments, SF of the medium surrounding the molecule (i.e., the cluster) is inferred from the rotational spectrum of the dopant. Specifically, the observed decoupling of the rotation of the molecule from that of the cluster signals the onset of SF in the cluster. The experimental setting commonly adopted in this kind of investigation is sketched in Fig. 1. Clusters of various sizes, comprising as few as a handful of atoms, are produced by expanding in vacuum through a small nozzle helium gas at high pressure. The evaporation that takes place on the cluster

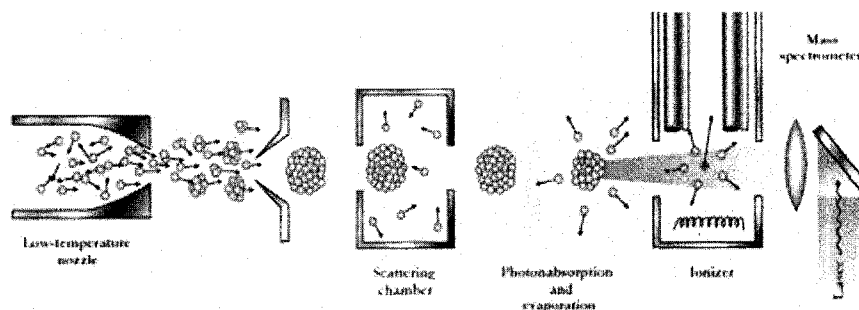


Figure 1: Schematic diagram of a HENDI spectroscopy experimental apparatus. [Reprinted with permission from Ref. [21]].

surface reduces the temperature of the cluster from approximately 30 K to less than 1 K, at which point the cluster enters the scattering chamber where a foreign molecule is captured. Finally, the molecule is spectroscopically activated by some suitable radiation. The absorbed photon results in a successive evaporation of helium atoms (beam depletion) detected by the mass spectrometer.

Fig. 2 shows the infrared spectra of a linear carbonyl sulfide (OCS) molecule surrounded by a cluster of helium at a temperature of 0.38 K [21]. When the cluster is made of ^4He atoms, the observed spectrum (panel *a*) shows a resolved rotational structure consistent with that of a free rotor, with a moment of inertia three times higher than that of the same dopant molecule in the gas phase. On the other hand, for a ^3He cluster (panel *b* of the same figure), the spectrum is consistent with that of a dopant in a normal fluid (the temperature of the experiment is in fact not sufficiently low to observe SF of ^3He), featuring a single, broad vibrational line. Moreover when the cluster is made of a $^3\text{He}/^4\text{He}$ mixture, resolved rotational lines reappear in the spectrum in the presence of as few as 64 ^4He atoms (panel *d*).

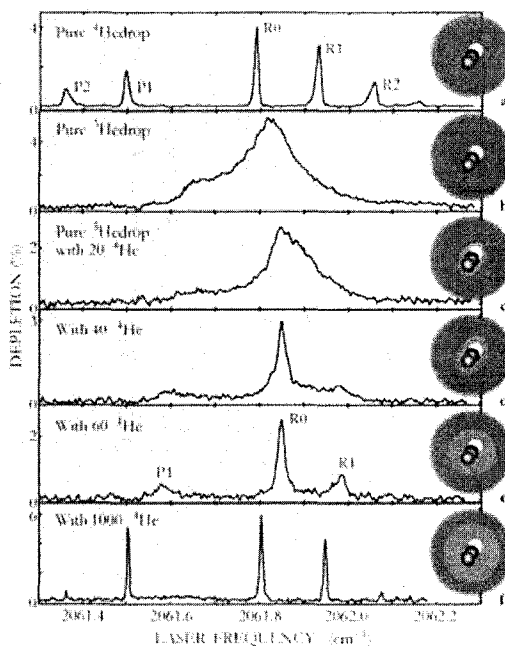


Figure 2: Infrared spectra of an OCS molecule embedded in a cluster of ^4He (a) and ^3He (b) atoms. Evolution of the spectrum in b when an increasing number of ^4He atoms is added (c-f). Temperature is 0.38 K. [Reprinted with permission from Ref. [21]].

The described behavior indicates, in the spirit of the Andronikashvili experiment [6], the superfluid character of the ^4He cluster, within which the embedded OCS molecule can rotate as though it were essentially in vacuo. An analogous experiment gave some evidence of a possible superfluid response of clusters of $N=14-16$ $p\text{-H}_2$ molecules surrounding the same impurity; these clusters were enclosed in a larger helium droplet. The same experiment failed to detect superfluid behavior of $o\text{-D}_2$ clusters [22].

These observations constitute the starting point for an intense theoretical ef-

fort, spanning now almost a decade, aimed at gaining a deeper understanding of SF in clusters of $p\text{-H}_2$ and, possibly, $o\text{-D}_2$ molecules. Quantum Monte Carlo (QMC) methods have quickly emerged as the most powerful theoretical tool to attack such an interesting problem, and have already been successfully employed to characterize the structure and SF of doped ^4He clusters both at finite and zero temperature [23, 24, 25, 26, 27]. For instance, Path Integral Monte Carlo (PIMC) simulations have yielded evidence of SF in $(p\text{-H}_2)_N$ clusters seeded with an OCS molecule [$\text{OCS}@ (p\text{-H}_2)_N$], for $10 \leq N \leq 17$, as well as in smaller complexes such as $\text{OCS}@ (p\text{-H}_2)_5$ and $\text{OCS}@ (o\text{-D}_2)_5$ [28, 29, 30]. Reptation Quantum Monte Carlo simulations have provided information about the structure of $\text{CO}@ (p\text{-H}_2)_N$, for $N \sim 12$, and have clarified some features of the experimentally measured infrared spectra [31, 32].

Obviously, of crucial importance to the full characterization of the experiments, as well as to the understanding of the microscopic origin of SF, remains the study of pristine (i.e., undoped) clusters. In this sense, hydrogen is even richer a playground than helium. For example, pure clusters of $p\text{-H}_2$ or $o\text{-D}_2$ provide a unique opportunity to study the effect of mass on the superfluid and structural properties of such small systems, because the $o\text{-D}_2$ molecular mass is twice that of $p\text{-H}_2$, while the intermolecular interaction is very nearly the same [33]. A mixed cluster of $p\text{-H}_2$ and $o\text{-D}_2$ molecules constitutes a simple realization of a mixture of isotopic bosonic molecules that offer the possibility to investigate other fundamental questions, e.g., the sensitivity of the superfluid response of a finite cluster to its detailed isotopic composition. Moreover, because the equilibrium phase of hydrogen is crystalline at low T , studying clusters of molecular hydrogen offers insight into the evolution of the physical properties as the number of particles is increased.

Although experimental data are not yet available, a novel technique, based on Raman spectroscopy, allowing one to assign spectral features to $(p\text{-H}_2)_N$ clusters with $N=2,\dots,8$ as well as to identify clusters featuring enhanced stability, seems to be a promising avenue for the study of superfluidity in pure or isotopically doped clusters [34].

The first numerical investigation of the physics of pure $p\text{-H}_2$ clusters at finite temperature, based on PIMC simulations, was published in 1991; it was restricted to three cluster sizes, namely $N=13, 18$ and 33 . Two clusters were found superfluid and “liquid-like”, while $(p\text{-H}_2)_{33}$ was observed to be “solid-like” at $T \leq 2$ K [35]. The same technique has been employed to study $p\text{-H}_2$ - $o\text{-D}_2$ mixtures down to $T=2.5$ K, but without including quantum exchanges [36]. No other studies of SF in pristine hydrogen clusters had been reported until 2006.

This thesis is a contribution to the theoretical investigation of the superfluid properties of pristine and isotopically doped clusters of hydrogen molecules. Our aim was to gain quantitative insight into the physics of these systems, by carrying out a systematic theoretical study, based on QMC simulations, with the ultimate goal of addressing fundamental scientific open questions such as:

- What is the mechanism responsible for the onset of SF in small clusters?
- What is the relation between their structural and superfluid properties?
- How does the physics of a finite hydrogen cluster approach that of the bulk, as the size of the cluster is increased?
- What is the dependence of the properties of these systems on the mass of the cluster components and on the intermolecular model interaction utilized?

- How do substitutional isotopic molecules change the behavior of a superfluid p -H₂ cluster?
- Is SF (if present) confined to a specific region (i.e. the surface) of a pristine cluster?
- What is the connection between global and local properties of a small cluster?

The relevance of these aspects goes obviously beyond the physics of molecular hydrogen clusters, as it impacts our general theoretical understanding of SF, perhaps the most fascinating macroscopic manifestation of quantum mechanics. When the research project whose results are reported here began, in late 2004, there was neither a systematic theoretical study of the structural and superfluid properties of pure p -H₂ and o -D₂ clusters as a function of size and temperature, nor any prediction, based on a fully quantum-mechanical treatment, for isotopically doped hydrogen clusters.

The QMC scheme employed in our calculations is the recently developed Continuous-space Worm Algorithm (WA) [37, 38]. This computational methodology allows one to perform essentially *exact* numerical calculations of thermodynamic properties of Bose systems. In particular, the superfluid fraction can be calculated with much greater accuracy and at much lower temperature than that afforded by conventional PIMC, which has been one of the leading many-body computational methods for the last 20 years [39]. Specifically, we have computed energetics, density profiles, three-dimensional structure and superfluid fraction of pure p -H₂ and o -D₂ clusters, as well as of isotopically doped hydrogen cluster of size as large as $N=48$ molecules, in the temperature range $0.0625 \text{ K} \leq T \leq 4 \text{ K}$.

Our main findings are briefly and schematically summarized as follows:

1) Pristine ($p\text{-H}_2$) $_N$ clusters with $N \leq 21$ below $T=1$ K are superfluid, and liquid-like, with a superfluid fraction $\rho_S \simeq 1$. On increasing the cluster size, ρ_S changes in a non monotonic fashion, reflecting important structural changes that occur on adding even a single molecule. For example, the addition of one molecule to an almost entirely superfluid cluster can result in the complete depletion of ρ_S , with the concomitant emergence of a remarkably solid-like structure. Moreover, some clusters display coexistence of insulating (solid-like), superfluid (liquid-like) phases, the latter induced by quantum exchanges and zero-point motion, becoming dominant as T is lowered. We refer to this behavior as *quantum melting* [40, 41].

2) Superfluid behavior has also been detected in $o\text{-D}_2$ clusters of about 14 molecules at $T=0.5$ K. The larger mass of the $o\text{-D}_2$ molecule renders a $o\text{-D}_2$ cluster generally more rigid than a $p\text{-H}_2$ one comprising the same number of molecules; however, also in the case of $o\text{-D}_2$ clusters superfluid response and structure strongly depend on the cluster size.

3) For both isotopes, we have observed (magic) clusters which feature enhanced stability. This property may reflect particular solid-like behavior as in the case of the cluster ($p\text{-H}_2$) $_{26}$ at $T=1$ K or the completion of a shell of molecules as for the system ($p\text{-H}_2$) $_{13}$ which does not rule out liquid-like behavior [41].

4) Substitution of $p\text{-H}_2$ with $o\text{-D}_2$ molecules, generally causes pristine superfluid $p\text{-H}_2$ clusters to turn progressively solid-like, their structure increasingly mimicking that of pure $o\text{-D}_2$ clusters with the same numbers of molecules. For clusters comprising more than 20 molecules, however, the change from liquid to solid-like can occur abruptly. A much smaller reduction of the superfluid response is observed if substitutional impurities are *ortho*-hydrogen ($o\text{-H}_2$) molecules [($o\text{-H}_2$) is another isotope, which has the same mass of $p\text{-H}_2$, but different spin ($S=1$)]. A

crucial observation is that few substitutional o -D₂ molecules sit in the inner part of the cluster, whereas o -H₂ impurities are primarily located near its surface.

5) Evidence of spatial segregation of the two isotopes is obtained for clusters with equal numbers of p -H₂ and o -D₂ molecules, of size up to 20 molecules altogether. The structure of these clusters is prevalently solid-like, and their superfluid response generally not significant down to $T=0.5$ K.

6) Our results for the local superfluid response of pristine p -H₂ clusters not only confirm the relation between SF and exchanges of molecules in different regions of the cluster but also give additional insight on how SF is distributed across the system. In fact it is shown that, contrary to what stated in a recent publication [42], SF is *not* localized at the surface; rather, in the low temperature limit clusters are *uniformly* superfluid; this statement applies not only to the more liquid-like ones (i.e., those with fewer than ~ 20 molecules), but also to those displaying a more pronounced shell structure, which softens at low temperature due to quantum melting, in turn underlain by exchange cycles involving molecules in both the inner and outer shells. Based on these results we contend that the physical picture proposed in Ref. [42] of SF as arising from “loosely bound surface molecules” does not apply. Indeed, we have observed no clusters with a rigid core and a superfluid outer shell. Instead, SF crucially depends on the onset of long exchange cycles involving *all* molecules, not just those on the surface [43].

All of the above findings generally underscore the prominent role played by long exchanges, especially involving molecules in different shells of the cluster, in stabilizing a liquid-like structure of large clusters at low T , in turn allowing for SF to occur [44].

We have performed calculations using three different interaction potentials namely

the Silvera-Goldman potential [45], the Buck [46], and the Lennard-Jones one. Although we observed some noticeable quantitative discrepancies between results obtained with different model interactions [47], only the energetics and the temperature scales depend on the potential utilized. On the other hand, all the qualitative physical conclusions are not affected by the choice of the intermolecular interaction.

The remainder of this thesis is organized as follows:

- in the first chapter we introduce the physical model adopted to describe our systems of interest and discuss in details the numerical method utilized for our calculations;
- in the second chapter we present and discuss our results;
- finally we outline our conclusions, also indicating possible avenues for further investigations.

Chapter 1

PHYSICAL MODEL AND METHODOLOGY

In this chapter we discuss the physical model and the methodology adopted to investigate, by means of Path Integral Monte Carlo (PIMC) computer simulations based on the Continuous-space Worm Algorithm (WA) [37, 38], the structural and superfluid properties of molecular hydrogen clusters.

1.1 Many-body Hamiltonian

If one seeks to carry out a microscopic study of molecular hydrogen clusters at low temperature, the starting point is a quantum-mechanical many-body Hamiltonian, making use of a realistic, *ab initio* potential to describe the interaction among particles. A hydrogen molecule can be treated as an individual particle (i.e., neglecting the electronic degrees of freedom). This approximation is largely justified being the energy associated to the first excited state of the order of one

electronvolt (~ 11600 K); therefore at the temperatures relevant to our study (of the order of 1 K) molecules can be considered in the electronic ground state (Born-Oppenheimer approximation). With 2 electrons in the $1s$ orbital a hydrogen molecule is to an excellent degree of approximation a spherically symmetric bound state, consequently, the intermolecular interaction can be described by means of a *central* potential. Quantum mechanics is necessary for this problem, as the thermal wavelength of a hydrogen molecule at temperatures below 1 K is of the same order of magnitude as that of a helium atom, i.e., a large overlap exists between the probability “clouds” of different particles. Thus, quantum-mechanical effects such as zero-point motion and exchanges of particles are expected to be just as important as in condensed helium.

We model our system of interest, as a collection of N p -H₂ (o -D₂) molecules, regarded as spin-0 point particles. If we assume for simplicity that all N particles in the cluster are identical, the Hamiltonian of the system can be written as¹:

$$H = -\lambda \sum_i^N \nabla_i^2 + V(\mathbf{R}) \quad (1.1)$$

where $\lambda = \hbar^2/2m = 12.031 \text{ K}\text{\AA}^2$ for p -H₂ (half of this value for o -D₂), $\mathbf{R} \equiv \mathbf{r}_1, \mathbf{r}_2 \cdots \mathbf{r}_N$ is a collective coordinate referring to all the N particles in the system, and $V(\mathbf{R})$ the total potential energy of interaction of the system corresponding to the many-particle configuration \mathbf{R} . The potential energy V is given by a sum of pairwise terms (three-body terms can be incorporated in part as *effective* pairwise contributions [45], while higher many-body interactions are neglected). As mentioned above the pair potential utilized is *central*, i.e., it depends on the relative

¹The expression of the hamiltonian of a p -H₂- o -D₂ mixed cluster is a straightforward generalization of (1.1).

distance of two molecules [see Eq. (1.2)]. In this work, therefore, it is consistently

$$V(\mathbf{R}) = \sum_{i < j} v(\|\mathbf{r}_i - \mathbf{r}_j\|). \quad (1.2)$$

Despite its apparent simplicity, an analytical solution of the Schroedinger equation based on the hamiltonian in (1.1) is out of question for clusters comprising more than two molecules. Hence the only viable computational strategy is tackling the problem numerically.

1.2 Computational methods

Quantum Monte Carlo techniques afford accurate, in principle *exact* estimates of thermodynamic properties of Bose systems at finite or zero temperature. Zero-temperature QMC methods [48] such as Path Integral Ground State (PIGS), Diffusion and Reptation Monte Carlo (DMC and RMC, respectively) make use of similar strategies to obtain, starting from an initial trial wave function, the ground-state of the system by means of a projection procedure. In all these methods, the trial wave function is chosen to capture the essential physics of the system, and is optimized with respect to various free parameters, according to the variational principle. In principle, methods such as PIGS and RMC [49] can “extract” the exact ground-state of the system, the only requirement on the trial wave function being that it be non-orthogonal to the true ground-state. In practice, the efficiency of these methods varies enormously, depending on the accuracy of the trial wave function; therefore, its optimization is a very important, often time-consuming part of the study. PIGS, RMC and DMC methods have been extensively employed in

the study of doped and pristine hydrogen clusters [31, 32, 50, 51, 52]. They have provided valuable results, not only to compare to experimental data available for clusters doped with a single impurity, but also to assign spectral features of the roto-vibrational spectrum of doped clusters to system of specific sizes [32]. A typical experimental spectrum, in fact, consists of several lines due to clusters of various sizes; the correct assignment of this lines is, in general, a very tough task to accomplish experimentally and becomes extremely difficult for large clusters.

Since we were interested in the study of structural and superfluid properties of molecular hydrogen clusters as a function of temperature T and cluster size N , the computational method for our investigation had to allow finite temperature simulations of systems of a given size (i.e., in the canonical ensemble). This is the specific case of PIMC (the only *exact* QMC method at finite temperature) which, therefore, has been our method of choice. In particular we used an implementation of this method based on the Continuous-space Worm Algorithm which, for a Bose system, such as a molecular hydrogen cluster, affords the calculation of key quantities (i.e., global and local superfluid fraction) with much greater accuracy [37, 38] than that provided by conventional PIMC [39].

1.3 Potentials

The computational methodology that we describe below, namely the Worm Algorithm, is formally exact². The only source of uncertainty in our study, is the model potential adopted, whose choice can obviously affect the reliability of the

²Statistical errors arising from the fact that one is using a Monte Carlo procedure can in practice be reduced to a point where they are essentially unnoticeable.

numerical estimates. This is the only input to the calculation³. As mentioned above, we have made use of spherically symmetric potentials only. It is worth mentioning that, in some applications, the spherical approximation for the interaction potential is regarded as rather poor, especially when studying systems in which hydrogen molecules interact with a foreign impurity (see, for instance, Ref. [53]). In such cases, a more elaborate pair potential may be needed, depending on the relative orientation of the two molecules as well. In our study however, we focus on *pristine* clusters, and thus do not expect our results to be significantly dependent on the spherical approximation for the pair interaction.

For the majority of our calculations we have used the Silvera-Goldman pair potential [45] which is employed in most of the published numerical work on molecular hydrogen clusters. Moreover, recent Quantum Monte Carlo studies have shown that the zero-temperature equation of state of bulk hydrogen computed with the Silvera-Goldman potential is in reasonable agreement with experiment [54, 55]. For comparison purposes, however, we have also obtained results using different intermolecular potentials, namely the Buck [46] and the Lennard-Jones (LJ) ones.

The Silvera-Goldman (SG) potential is expressed as:

$$v_{SG}(r) = \epsilon \left\{ e^{-\alpha - \beta r - \lambda r^2} - \left[\frac{A}{r^6} + \frac{B}{r^8} - \frac{D}{r^9} + \frac{C}{r^{10}} \right] f(r) \right\} \quad (1.3)$$

where the first term is the repulsive part, which arises from the Pauli exclusion principle, that prevents electrons in the orbital clouds of two different atoms or molecules from overlapping in space. The second term incorporates both the (van der Waals) long range attractive interaction of induced dipoles as well as a term

³It is worth stressing that the pair potential is *not* adjusted in our calculation.

(proportional to r^{-9}) which effectively describes three-body interactions of the Axilrod-Teller-Muto form. The damping function f , whose role is to turn the long-range interaction off at short distances, is given by:

$$f(r) = \exp\left[-\left(\frac{r^*}{r} - 1\right)^2\right] \quad \text{if } r < r^*, \quad 1 \text{ otherwise.} \quad (1.4)$$

There are altogether nine parameters in the above expression, whose values are provided in Ref. [45]. The Buck potential has the same analytic form as the SG but with $D = 0$, i.e., it does not include three-body contributions (obviously the values of the parameters are different). Finally, the simple LJ potential is expressed as follows:

$$v_{LJ}(r) = 4\varepsilon\left[\left(\frac{\sigma}{r}\right)^{12} - \left(\frac{\sigma}{r}\right)^6\right] \quad (1.5)$$

where σ is the effective molecular diameter and ε the attractive well depth. For $p\text{-H}_2$, the values of these parameters adopted in previous numerical works (see for example Refs. [36, 42]) are $\sigma=2.96 \text{ \AA}$, and $\varepsilon=34.16 \text{ K}$.

The LJ is perhaps the most popular model interaction, extensively utilized in simulations of both classical and quantum fluids and solids. Its main quality is its simplicity, and the fact that it does incorporate the most important physical features of any interatomic or intermolecular interaction. It is rather crude, though, and the agreement that it affords with experiment is typically not very good. The most obvious shortcoming is the unphysical divergence at short distances, which renders it particularly “stiff”; however, as clearly shown in Fig. 1.1, even at long distances it fails to provide a quantitative description of the pair interaction. In Fig 1.1 we compare the three potential. For short distances (not shown for clarity) the LJ potential is the most repulsive. In fact, its analytical form displays

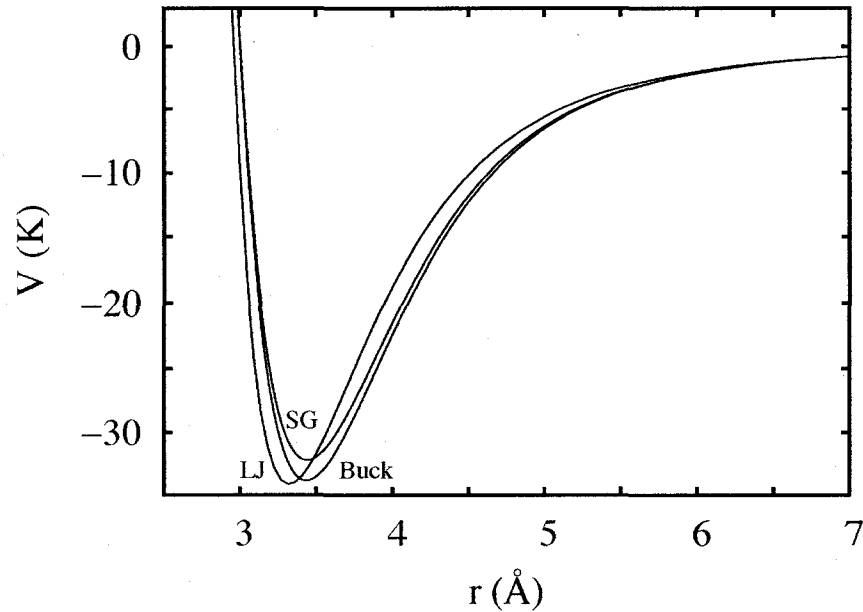


Figure 1.1: Functional form of the Buck, LJ and SG potential.

an unphysical divergence at $r=0$, not present in the expression of the SG (or Buck) potential. Aside from a small region around the minimum, the LJ potential is far less attractive than the SG and the Buck potentials, the latter being the most attractive of the three. These features cause, as we shall see, important discrepancies between numerical estimates of main physical quantities computed with different potentials.

Next we review the foundations of Feynman's Path Integral approach to quantum statistical mechanics and discuss in details the numerical method adopted for

our calculations.

1.4 Path Integrals

Consider a system of N identical, interacting quantum particles of mass m . We shall initially neglect for simplicity quantum statistics, i.e., assume that the particles are identical but *distinguishable*. Later on we shall incorporate indistinguishability (and Bose statistics) in the formalism. Let the quantum-mechanical Hamiltonian of the system be given by an expression such as (1.1), namely

$$\hat{H} = \hat{H}_0 + \hat{V} \quad (1.6)$$

where

$$\hat{H}_0 = -\lambda \sum_i^N \nabla_i^2 \quad \text{and} \quad \hat{V} = V(\mathbf{R}) \quad (1.7)$$

with the notation introduced in section 1.1. As previously explained, in our study the potential energy of interaction V is expressed as a sum of terms describing the interactions between pairs of particles. However, the formalism described below does not depend on the detailed form of $V(\mathbf{R})$. Henceforth, we shall assume for definiteness that the many-particle system of interest is three-dimensional.

The thermal average of a quantum-mechanical operator \hat{O} (assumed for simplicity diagonal in the coordinates space) at a temperature $T = 1/\beta$ (in our notation, we set the Boltzmann constant $k_B=1$ and measure all energies in K) is given by:

$$\langle O \rangle = \frac{1}{Z} \int d\mathbf{R} O(\mathbf{R}) \rho(\mathbf{R}, \mathbf{R}, \beta) \quad (1.8)$$

where

$$\rho(\mathbf{R}, \mathbf{R}, \beta) = \langle \mathbf{R} | e^{-\beta \hat{H}} | \mathbf{R} \rangle \quad (1.9)$$

is the many-body density matrix and

$$Z = \int d\mathbf{R} \rho(\mathbf{R}, \mathbf{R}, \beta) \quad (1.10)$$

is the *canonical partition function*. Aside from a few simple cases, an analytical expression for the many-body density matrix of an interacting system is generally unknown, as its calculation would require the knowledge of the full spectrum of the many-body Hamiltonian \hat{H} . However, a systematic procedure exists, first proposed by R. P. Feynman, to recover the full ρ [56].

Specifically, one begins from the formal identity:

$$e^{-\beta \hat{H}} \equiv \left(e^{-\tau \hat{H}} \right)^M \quad \text{with} \quad \beta = M\tau; \quad (1.11)$$

on taking advantage of the completeness relation

$$\int d\mathbf{R} |\mathbf{R}\rangle \langle \mathbf{R}| \equiv 1 \quad (1.12)$$

and on introducing M such identity operators between all consecutive exponentials in (1.11), one obtains

$$\begin{aligned} \rho(\mathbf{R}, \mathbf{R}, \beta) &= \langle \mathbf{R} | e^{-\tau \hat{H}} e^{-\tau \hat{H}} \dots e^{-\tau \hat{H}} | \mathbf{R} \rangle = \\ &= \int d\mathbf{R}_1 \dots d\mathbf{R}_{M-1} \rho(\mathbf{R}, \mathbf{R}_1, \tau) \dots \rho(\mathbf{R}_{M-1}, \mathbf{R}, \tau), \end{aligned} \quad (1.13)$$

still formally exact for arbitrary M . If $M \gg 1$, then the inverse temperature

argument τ in the density matrices inside the multidimensional integral becomes small; in this limit, $\rho(\mathbf{R}, \mathbf{R}', \tau)$ can be approximated as follows:

$$\rho(\mathbf{R}, \mathbf{R}', \tau) \approx \rho_F(\mathbf{R}, \mathbf{R}', \tau) \exp\left[-\tau\left(V(\mathbf{R}) + V(\mathbf{R}')\right)/2\right] + \mathcal{O}(\tau^3) \quad (1.14)$$

where

$$\rho_F(\mathbf{R}, \mathbf{R}', \tau) = \langle \mathbf{R} | e^{-\tau \hat{H}_0} | \mathbf{R}' \rangle = \prod_{j=1}^N \rho_f(\mathbf{r}_j, \mathbf{r}'_j, \tau) \quad (1.15)$$

having defined

$$\rho_f(\mathbf{r}, \mathbf{r}', \tau) = \frac{1}{(\sqrt{4\pi\lambda\tau})^3} \exp\left[-\frac{|\mathbf{r} - \mathbf{r}'|^2}{4\lambda\tau}\right]. \quad (1.16)$$

Expression (1.15) is the density matrix for a system of non-interacting, identical (but distinguishable) quantum particles [56]. Eq. (1.14) can be easily verified by expanding the exact ρ to second order in τ . On plugging the approximate expression (1.14) into the basic equation (1.8), one obtains an approximation for thermal expectation values, as a ratio of multidimensional ($3NM$ dimensions) integrals, which may not be easily computable in practice, but can be rendered arbitrarily accurate on taking M large. Indeed, it can be formally shown that this procedure will yield an *exact* thermal expectation value in the limit $M \rightarrow \infty$ (i.e., $\tau \rightarrow 0$) [56], wherein (1.8) is transformed into the following:

$$\langle O \rangle = \frac{\int \mathcal{D}\mathbf{R}(\tau) O(\mathbf{R}(\tau)) \exp[-\mathcal{S}[\mathbf{R}(\tau)]]}{\int \mathcal{D}\mathbf{R}(\tau) \exp[-\mathcal{S}[\mathbf{R}(\tau)]]} \quad (1.17)$$

where the integrations run over all possible, *continuous* many-particle “paths” $\mathbf{R}(\tau)$, with $0 \leq \tau \leq \beta$ and $\mathbf{R}(\beta) = \mathbf{R}(0)$. The quantity τ is normally referred to as *imaginary time*, owing to the formal equivalence of the operator $\exp[-\tau \hat{H}]$ to

a quantum-mechanical imaginary-time evolution operator. Finally, $S[\mathbf{R}(\tau)]$ is the so-called *Euclidean action*

$$S[\mathbf{R}(\tau)] = \int_0^\beta d\tau \left\{ \frac{m}{2} \sum_{i=1}^N \left(\frac{d\mathbf{r}_i}{d\tau} \right)^2 + V(\mathbf{R}(\tau)) \right\} \quad (1.18)$$

which differs from the classical action by the sign of the potential energy term.

1.4.1 Quantum statistics

If particles in the system are now assumed to be *indistinguishable*, and obey either Bose or Fermi statistics, the above formalism must be modified to ensure that the many-body density matrix feature the proper symmetry upon interchange of the particle labels. We shall henceforth assume that particles obey *Bose statistics*, as that is the situation that we face in this study.

It is simple to show that the above path integral formalism remains valid, the only modification being that many-particle paths must be allowed to end at $\tau = \beta$ with the same positions of all particles as at $\tau = 0$, but with a possible *permutation* of the labels of the particles, i.e., $\mathbf{R}(\beta) = P\mathbf{R}(0)$, where P is a permutation of particle indices. In other words, for example, the position of particle 1 at $\tau = \beta$ may be that of particle 5, say, at $\tau = 0$ and so on.

The inclusion of such permutations is crucial in order to capture effects due to quantum (Bose) statistics, including (and chiefly) superfluidity [39].

1.4.2 Numerical implementation

Formally, one can evaluate thermal expectation values based on the prescription (1.17) by computing the numerator and denominator for a finite number M of

“time steps”, using the “high-temperature” approximation (1.14) for $\rho(\mathbf{R}, \mathbf{R}', \tau)$ (different approximations exist, enjoying faster convergence with τ ; we shall come back to this point later on), and then taking the limit of the ratio for $M \rightarrow \infty$. Unfortunately, the analytical evaluation of the integrals appearing at both numerator and denominator of expression (1.17) is out of question for all but the simplest many-body problems, as the presence of pairwise interactions does *not* allow one to factorise integrations. For this reason, the path integral formalism only yielded *qualitative*, even if interesting, insight for about thirty years since its formulation. All of that changed with the appearance of large-scale computing facilities, that allow one to carry out the computational program described above *numerically*. The only viable strategy to perform a numerical evaluation of (1.17), is one based on Monte Carlo. The presence of a very large number of variables ($3NM$ in three dimensions, with N and M possibly as large as several thousands, for different reasons each), renders a straightforward numerical integration by discretization unfeasible, given the exponential scaling of computer resources needed as a function of the number of variables.

Path Integral Monte Carlo

We begin by re-writing (1.17) assuming a finite number M of steps:

$$\langle O \rangle \approx \frac{\int d\mathbf{X} O(\mathbf{X}) P(\mathbf{X})}{\int d\mathbf{X} P(\mathbf{X})} \quad (1.19)$$

where $\mathbf{X} = \{\mathbf{R}_0, \mathbf{R}_1, \dots, \mathbf{R}_{M-1}, \mathbf{R}_M\}$ is a many-particle path (a collection of configurations \mathbf{R}_i visited by the system at the discrete “imaginary times” $0, \tau, \dots, M\tau = \beta$; each path consists of N single-particle paths (also referred to as *world lines*). A

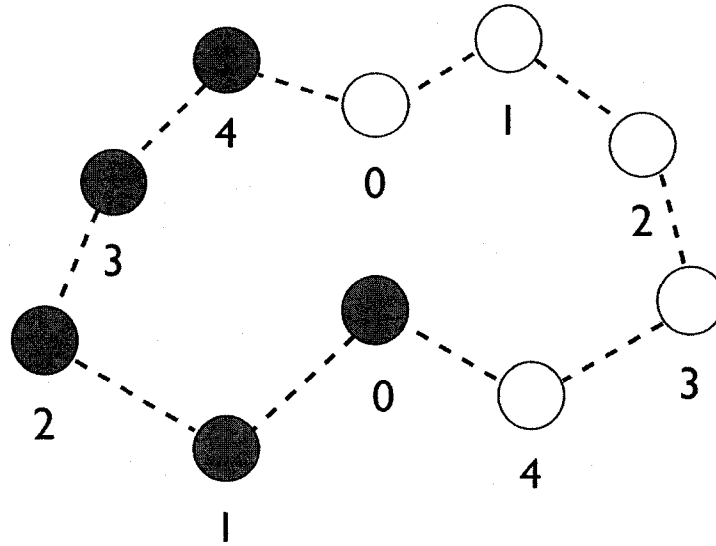


Figure 1.2: Schematic representation of the paths of two particles in imaginary time. In this example, $M=5$, and the two particles undergo an exchange.

world line is a sequence of M linked beads (positions), labeled by the index of the corresponding imaginary-time slice (see Fig. 1.2).

As mentioned above, paths are periodic in imaginary time, i.e., it must be $\mathbf{R}_M = P(\mathbf{R}_0)$, meaning that the positions of all particles at “slices” M and 0 must be identical, but a permutation P of particles is allowed, on account of their indistinguishability.

We can generally write

$$P(\mathbf{X}) = e^{-U(\mathbf{X})} \prod_{i=0}^{M-1} \rho_F(\mathbf{R}_i, \mathbf{R}_{i+1}, \tau) \quad (1.20)$$

where U is a function that includes correlations both in space and imaginary time

rising from the interaction among particles. If the simple approximation (1.14) is adopted, then

$$U(\mathbf{X}) = \tau \sum_{j=0}^{M-1} V(\mathbf{R}_j) \quad (1.21)$$

but several choices are possible, and indeed the one that we use in this work is not (1.21). The only requirement is that, whatever “high-temperature” approximation one chooses, the proper limit is recovered [i.e., expression (1.17)] as $M \rightarrow \infty$ (i.e., $\tau \rightarrow 0$).

As mentioned above, one can carry out the multi-dimensional integration in (1.19) numerically, using the Monte Carlo method. The ensuing methodology is known as Path Integral Monte Carlo (PIMC). A Monte Carlo evaluation of the integral (1.19) consists of generating on a computer, a large number N_P of independent many-particle paths $\{\mathbf{X}_i\}$ ($i=1, \dots, N_P$) randomly drawn from the probability distribution $P(\mathbf{X})$. The thermal average in (1.19) can be estimated as the statistical average of the observable \hat{O} over the set of paths. A key ingredient to the scheme, like in any Monte Carlo scheme, is the efficient generation of *pseudo-random numbers*, a task for which very well-established procedures exist, as this has been a subject of intense study in applied mathematics over the past five decades [57].

1.5 Metropolis algorithm

The set of paths $\{\mathbf{X}_i\}$ can be generated by means of the Metropolis algorithm [58]. The idea is to produce a random walk through the space of the many-particle paths, based on a fundamental transition probability $\mathcal{P}(\mathbf{X} \rightarrow \mathbf{X}')$, with an arbitrary initial condition \mathbf{X}_0 . The goal is that of “visiting” the generic path \mathbf{X} with a probability proportional to $P(\mathbf{X})$. A fundamental requirement for the

random walk is that of *ergodicity*, i.e., for each visited point there has to be a finite time of return to the same point, at least in principle.

Such a random walk is markovian because $\mathcal{P}(\mathbf{X} \rightarrow \mathbf{X}')$ depends only on the current position (in the configurational space), not on those previously visited. One way to accomplish the above goal, i.e., sample $P(\mathbf{X})$, is by fulfilling the so-called *detailed-balance* condition:

$$P(\mathbf{X})\mathcal{P}(\mathbf{X} \rightarrow \mathbf{X}') = P(\mathbf{X}')\mathcal{P}(\mathbf{X}' \rightarrow \mathbf{X}). \quad (1.22)$$

The Metropolis algorithm accomplishes the above by factoring the transition probability \mathcal{P} as

$$\mathcal{P}(\mathbf{X} \rightarrow \mathbf{X}') = S(\mathbf{X} \rightarrow \mathbf{X}') A(\mathbf{X} \rightarrow \mathbf{X}'). \quad (1.23)$$

Here, $S(\mathbf{X} \rightarrow \mathbf{X}')$ is an arbitrarily chosen sampling probability, whereas A is an *acceptance probability*, given by:

$$A(\mathbf{X} \rightarrow \mathbf{X}') = \min \left\{ 1, \frac{P(\mathbf{X}') S(\mathbf{X}' \rightarrow \mathbf{X})}{P(\mathbf{X}) S(\mathbf{X} \rightarrow \mathbf{X}')} \right\}. \quad (1.24)$$

Although, as mentioned above, the choice of the *sampling* probability is arbitrary, S should be a simple distribution that can be sampled efficiently. We summarize below the procedure to sample, using the Metropolis algorithm, the distribution probability P ;

- the random walk starts from an arbitrary initial point (i.e., a path) \mathbf{X}_0 ;
- let \mathbf{X}_j be the current position of the random walk. A *trial* new path \mathbf{X}_k is sampled by updating the positions of one or more particle at several imaginary-time slices, with probability $S(\mathbf{X}_j \rightarrow \mathbf{X}_k)$;

- compute the acceptance probability $A(\mathbf{X}_j \rightarrow \mathbf{X}_k)$;
- draw a random number η uniformly distributed in $[0,1)$; if $A > \eta$, then the next point of the sequence is $\mathbf{X}_{j+1} \equiv \mathbf{X}_k$; otherwise, $\mathbf{X}_{j+1} \equiv \mathbf{X}_j$.

The above scheme is fairly general, and its simplest implementation is rather straightforward. However, whether or not an actual calculation will be feasible in practice, given the computational resources that are available, crucially depends on the efficiency of the scheme. In particular, the strategy employed to update the many-particle paths, embodied in the sampling probability S , is of crucial importance to the overall efficiency of the calculation; independent implementations of PIMC proposed over the past two decades [39] differ ultimately in the choice of S . In this work, we have made use of a recently formulated PIMC scheme, known as Worm Algorithm, which has afforded a significant efficiency boost over existing PIMC strategies [37, 38]. Among other things, this means that one can study Bose systems comprising as much as three order of magnitude more particles, and at a temperature an order of magnitude lower than previously possible.

1.6 Continuous-space Worm Algorithm

The main difference between the WA and conventional PIMC, is the structure of the configurational space. In the conventional approach the configurational space contains only closed paths, each representing one particle. On the other hand, the WA operates in an extended configurational space containing configurations in which all the world lines are closed (Z -sector) as well as configurations in which one world line is open (G -sector). Such a special open path, whose head and tail

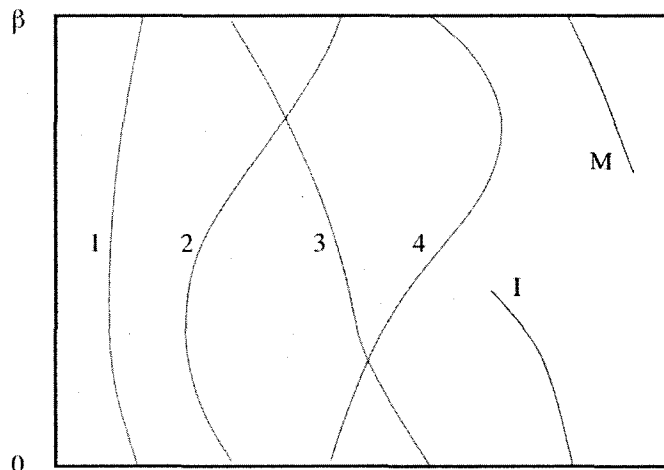


Figure 1.3: Schematic representation of one configuration in the G -sector, for a system of five particles in one dimension. This configuration contains four closed and one open world line, namely the worm, whose head (I) and tail (M) are indicated in picture.

can move in imaginary time, is called “worm”. A schematic representation of a configuration in the G -sector is presented in Fig.1.3.

The transition between the Z - and G - sector (and vice-versa) takes place by opening (closing) a closed (open) world line. When the worm is created, two special beads appear, namely the head and the tail of the worm, to which we refer for historical reason as *Ira* and *Masha*. The thermodynamic expectation values of the physical observables (except for the Matsubara Green function and the one-body density matrix) are computed in the Z -sector of the configurational space, i.e., the one with no worm, which is the full configurational space of conventional PIMC.

The general WA described in Refs. [37, 38] allows one to perform simulations in the *grand-canonical* ensemble, in which the number of particles fluctuate and the chemical potential is given as input, in lieu of the density. Grand-canonical simulations are performed by allowing the worm to “disappear” as well as “appear” in the configuration. In this work, we have used a canonical implementation. The only difference with the fully grand-canonical version, is that all the Z -sector configurations have the same number of particle (there are no fluctuations in N). Moreover, G -sector configurations have always $N - 1$ closed world lines, plus the worm.

1.6.1 Metropolis updates

The generic configuration \mathbf{X} , i.e., a many-particle path with or without a worm, is assigned a statistical weight $W(\mathbf{X}, \tau)e^{-U(\mathbf{X})}$, with

$$W(\mathbf{X}, \tau) = \prod_{j=0}^{M-1} \rho_F(\mathbf{R}_j, \mathbf{R}_{j+1}, \tau) \quad (1.25)$$

where ρ_F given by (1.15). Obviously, for Z -sector configurations the weight coincides with $P(\mathbf{X})$ given by (1.20). The extended configuration space is sampled by means of elementary ergodic updates, defined in complementary pairs: *open/close*, *advance/recede*, *swap*; each of them involves the worm. The updates that change the number of continuous variables in imaginary time are arranged in complementary pairs, so as to ensure the requirement of the detailed balance. The swap update does not change the number of continuous variables and, in this sense, is self-complementary. Below, a detailed description of all these moves is provided. Henceforth, we shall be adopting a commonly used terminology and refer to the

the j th position (j ranging from 0 to $M - 1$) of, say, the i th particle along its path, as a “bead”.

Open

The **open** update is only possible when the random walk is at a configuration in the Z -sector. Starting from the many particle path \mathbf{X}_{old} one particle world line, say the i th, and an integer P (with $2 \leq P \leq P_{max} \leq M$ chosen at the beginning of the simulation and adjusted to yield the desired average acceptance for this move) are selected at random. All the *intermediate* beads of the path of this particle, from the $(M - P)$ th to the $(M - 1)$ th (with exclusion of the ends) are removed⁴. If the move is accepted, the selected world line will become the *worm*; the *Ira* bead will coincide with the $(M - P)$ th bead of the i th world line, while *Masha* will be at the $(M - 1)$ th bead of the same world line (without loss of generality *Masha* can be kept fixed at the last bead). The new configuration \mathbf{X}_{new} is accepted with probability:

$$A_{op} = \min \left\{ 1, \frac{e^{\Delta U}}{\rho_f(\mathbf{r}_I, \mathbf{r}_{M-1}, K\tau)} \right\} \quad (1.26)$$

where $\mathbf{r}_I, \mathbf{r}_{M-1}$ are the positions of the beads of *Ira* and *Masha*, $K = P - 1$ and, here and in the following, $\Delta U = U(\mathbf{X}_{old}) - U(\mathbf{X}_{new})$.

Close

The **close** update is only possible in the G -sector. If the number of slices between *Ira* and *Masha* in the positive direction of the imaginary time is K with $1 \leq K < P_{max}$ (otherwise the move cannot be attempted), $K - 1$ intermediate

⁴If $P = 2$ no beads are removed, only the link between the bead $M - 2$ and the bead $M - 1$.

new beads are sampled *directly* from the product of K free-particle propagators⁵

$$\prod_{j=1}^K \rho_f(\mathbf{r}_{j-1}, \mathbf{r}_j, \tau) \quad (1.27)$$

where $\mathbf{r}_0 \equiv \mathbf{r}_I$ and $\mathbf{r}_K \equiv \mathbf{r}_{M-1}$. The acceptance probability is given by:

$$A_{cl} = \min\{1, \rho_f(\mathbf{r}_I, \mathbf{r}_{M-1}, K\tau) e^{\Delta U}\}. \quad (1.28)$$

Advance/Recede

In the G -sector, the position of *Ira* can be updated by moving it backward or forward in imaginary time. Let I be the current position of *Ira* in imaginary time, i.e., $0 \leq I < M - 1$. In an *Advance* type update, a randomly chosen number $P \leq M - 1 - I$ of imaginary-time slices is sampled, and positions of beads generated by the direct sampling of free-particle propagators, as in *Close*. Conversely, the *Recede* update consists of erasing a random number H of beads, starting from I and going back in imaginary time⁶. With our notation, the acceptance probability of these two update is expressed by the same formula:

$$A_{ad(re)} = \min\{1, e^{\Delta U}\}. \quad (1.29)$$

⁵Gaussian probability distributions can be easily sampled directly using random numbers; see, for instance, Ref. [57].

⁶If *Ira* and *Masha* are already adjacent, no *Advance* (if $I=M-2$) or *Recede* (if $I=0$) move may be attempted. If $H > w - 2$ where w is the number of beads of the worm, *Recede* move is automatically rejected.

Swap

The **swap** update is the key update of the WA, as it allows for the efficient sampling of many-particle permutations which is crucial to obtain accurate estimates of the superfluid fraction. A schematic representation of a swap is illustrated in Fig. 1.4. This update involve one closed world line and the worm. Let Ira be on the j th

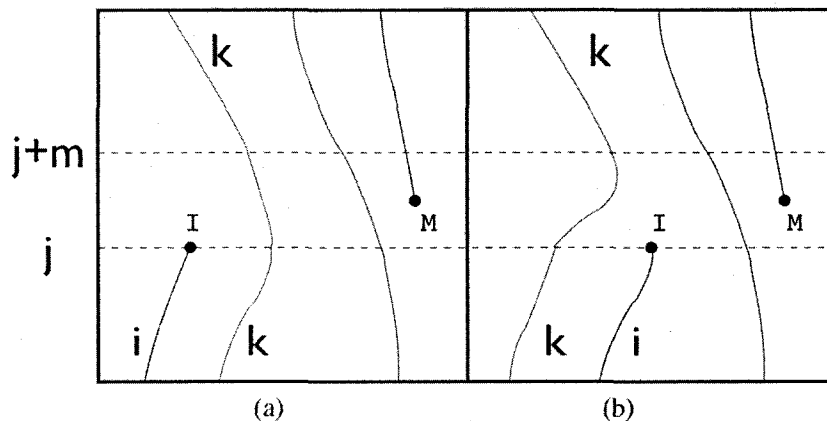


Figure 1.4: Configuration of three particles before (left) and after (right) a swap update.

slice of the i th world line, and let us select a random closed world line, as well as another time slice $j+m$, with $1 \leq m \leq Q_{max}$, $Q_{max} < M$ being a number chosen at the beginning of the simulation in order to yield the desired average acceptance for this move. The selection of the closed world line is done by sampling a probability table⁷ constructed with free-particle propagators:

$$\mathcal{T}_k = \frac{\rho_f(\mathbf{r}_{ij}, \mathbf{r}_{k,j+m}, m\tau)}{\sum_{l \neq i} \rho_f(\mathbf{r}_{ij}, \mathbf{r}_{l,j+m}, m\tau)} = \frac{\rho_f(\mathbf{r}_{ij}, \mathbf{r}_{k,j+m}, m\tau)}{\sum_i} \quad (1.30)$$

⁷The sampling of a discrete probability table \mathcal{T}_j requires that a single random number χ be drawn. The entry l that is selected is that for which $\sum_{j < l} \mathcal{T}_j \leq \chi \leq \sum_{j < (l+1)} \mathcal{T}_j$.

where \mathbf{r}_{lp} stands for the position of bead p of the l th world line. Once a specific world line k has been sampled (and clearly the table gives greater weight to world lines that go through the spatial vicinity of Ira), a set of intermediate beads, going from \mathbf{r}_{ij} to $\mathbf{r}_{k,j+m}$ (the end beads are left unchanged) is sampled from free-particle propagators, just like in the *Close* move. Contextually the beads $(j+1), \dots, (j+m-1)$ of the k th world line are erased. If the whole update is accepted, the world line j reconnects to the world line k , and the position of Ira changes as shown in figure. A straightforward relabeling of the beads from 1 to j of both the i th and k th world lines is required, as shown in Fig. 1.4⁸. The acceptance rate is given by:

$$A_{sw} = \min\left\{1, e^{\Delta U \frac{\sum_i}{\sum_k}}\right\}. \quad (1.31)$$

Permutation sampling

As mentioned before, sampling many-particle permutations is a crucial ingredient of any realistic quantum simulation strategy. It is precisely these exchange cycles that occur in Bose fluids at low temperature, which underlie macroscopic physical phenomena such as Bose-Einstein condensation and SF. The combination of moves described above represents a major step forward compared to the previous, accepted PIMC prescription [39], which suffers from an *exponential decrease* of efficiency of sampling of long permutation cycles, with increased number of particles and/or of imaginary-time slices M . The loss of efficiency occurs for the following reason: in conventional PIMC, the permutation of a group of particles is sampled by “cutting” the corresponding world lines and by attempting a reconnection, by “re-sewing” all open world lines in such a way that a permutation occurs, *all while*

⁸Obviously, care must be taken to ensure that the correct information about the *reconnection* of all world lines across the β -line be preserved.

remaining in the Z-sector. Such a procedure works reasonably well if particles interact only weakly; however, in the presence of an interaction potential with a repulsive core at short distances (featured by essentially *any* realistic interatomic or intermolecular model interaction), when the new pieces of world lines are constructed, no matter how cleverly, inevitably two or more particles will be brought in the vicinity of one another, with a large probability that the potential energy will be high, due to the presence of the repulsive core. This will cause a very high rate of rejection for permutational moves, especially when the group of particles in the permutation cycle is greater than two.

The ensuing inefficiency is particularly serious an issue when attempting to study SF, which is precisely underlain by long permutation cycles, involving a finite fraction of all the particles in the system. For this reason, and in spite of (at least) a hundredfold increase in computer speed since the pioneering work of Ref. [59] it has not proven possible to obtain, with the conventional PIMC scheme, estimates of the superfluid fraction, e.g., in bulk liquid ^4He , for finite systems of more than $N=64$ particles. Besides the unfavorable scaling of computing resources as a function of N , another major issue that this entails is the difficulty of assessing reliably whether the observed absence of long permutation cycles reflects a genuine physical effect, or merely lack of ergodicity of the path sampling scheme.

This hurdle is overcome in the WA, as the *Swap* move generates all possible many-body permutations through a chain of local single-particle updates. Since no two particles need be brought within a distance of the order of the hard core of a typical interatomic potential, this move enjoys a high acceptance rate, similar to that for the *Advance/Recede* updates. It must be emphasized that in the WA, unlike in conventional PIMC, arbitrary permutations of identical particles, as well as macro-

scopic exchange cycles need not be explicitly sampled. They *appear automatically*, if the physical conditions warrant them.

The WA has first been shown to afford the simulation of the superfluid transition in liquid ^4He in two and three dimensions, for systems comprising as many as 2500 particles, i.e., about 100 times greater than those accessible to conventional PIMC [37, 38]. Subsequently, it has been applied to the study of Bose condensation in crystalline ^4He in the presence of vacancies and extended defects such as grain boundaries and dislocations, for systems comprising as many as 10^4 particles [60, 61, 62, 63]. In all of these applications, the WA has provided accurate numerical results, simply not obtainable with any other existing method. It has to be stressed, however, that the WA is not merely about doing large system sizes (important as this is); it is also the first grand-canonical QMC method with local updates that incorporates in full quantum statistics. It affords the exact computation of imaginary-time off-diagonal correlations, such as the one-particle Matsubara Green function, that are not accessible to conventional PIMC (nor to any other QMC technique in continuous space).

In this work, the WA was applied to study finite systems with a relatively small number of particles, and one may therefore think that its usefulness may be somewhat more limited. This is not the case, however, as we shall see. Specifically, the much greater efficiency with which the WA can sample long permutation cycles, compared to traditional PIMC, has resulted in intriguing new physics being revealed.

1.7 Details of the simulation

We model our system of interest as a collection of N $p\text{-H}_2$ ($o\text{-D}_2$)⁹ molecules regarded as point particles (for details see section 1.1). The intermolecular interaction potential used for the majority of our calculations is the SG one whose analytic expression is reported in Eq. (1.3) [Buck and LJ interactions (see section 1.3) have been used as well for comparison]. In our calculations the system is enclosed in a cubic box with periodic boundary conditions in all directions. Because we are interested in studying a finite cluster, the box side is chosen sufficiently large (typically 50 Å) that the cluster is entirely contained in a region of size equal to less than half of the box size, thereby rendering the use of periodic boundary conditions immaterial (they are used for convenience only). In previous calculations (e.g., Ref. [35]), an artificial confining potential was adopted, in order to prevent molecules from evaporating (i.e., to keep the clusters together). We found this device unnecessary, as all the clusters studied here stay together, with no sign of evaporation, without such an external potential.

1.7.1 High-temperature density matrix

We outlined in 1.4.2 how several different high-temperature approximations for the many-body density matrix exist; all of them are constructed to recover the same limit, namely Eq. (1.17). The preference toward one or another form depends on a trade-off between the *efficiency* with which the approximate density matrix is computed (as that operation must be performed many times during a typical

⁹Extension to isotopic mixtures is straightforward once one takes into account the different masses.

simulation), and a fast convergence of the physical estimates vis-a-vis the number M of “slices” that is required. A particular form, known as the “pair-product”, became a rather popular choice since its introduction by Pollock and Ceperley [59], and was for a long time regarded as optimal. Its implementation and use are extremely cumbersome, however, and in recent times its real effectiveness and accuracy have been seriously questioned [64]. In this work, we have used a high-temperature approximation that is accurate up to the fourth order in the imaginary time τ [65]. Specifically the analytic expression for the function U in Eq. (1.20) that we employed is given by:

$$U(\mathbf{X}) = \frac{2\tau}{3} \sum_{j=0}^{M-1} \left[V(\mathbf{R}_j) + \tilde{V}(\mathbf{R}_j) \right] \quad (1.32)$$

where

$$\tilde{V}(\mathbf{R}_j) = \begin{cases} V(\mathbf{R}_j) + (\lambda\tau^2/3) \left[\sum_{i=1}^N (\nabla_i V(\mathbf{R}_j))^2 \right] & \text{odd } j \\ 0 & \text{even } j. \end{cases} \quad (1.33)$$

We empirically found the value $\tau = 1/640 \text{ K}^{-1}$ to yield estimates indistinguishable, within our quoted statistical uncertainties, from those extrapolated to the $\tau \rightarrow 0$ limit (i.e., the limit where the method becomes formally *exact*).

1.7.2 Thermodynamic estimators

In the present work we computed energetics, superfluid fraction ρ_S and profiles of total and superfluid density [$n(r)$ and $n_S(r)$ respectively]. The energy estimators utilized are discussed extensively in Ref. [65]. The average kinetic energy per

particle is given by:

$$\langle K \rangle \approx \frac{3}{2\tau} - \frac{1}{4\lambda\tau^2} \langle (\mathbf{r}_k - \mathbf{r}_{k+1})^2 \rangle + \frac{\lambda\tau^2}{9} \langle (\nabla V(\mathbf{R}_{2k}))^2 \rangle \quad (1.34)$$

where $\langle \dots \rangle$ stands for the thermal average, $(\mathbf{r}_k - \mathbf{r}_{k+1})^2$ is the square distance between the positions of a particle at adjacent time slices and the gradient in the third term is taken with respect to the coordinate of one of the particles at an even slice. The average potential energy per particle is obtained as:

$$\langle V \rangle \approx \frac{1}{N} \langle V(\mathbf{R}_{2k-1}) \rangle. \quad (1.35)$$

We computed the superfluid fraction by means of the “area estimator”. In a finite system, such as a small cluster, and within the PIMC formalism, it can be shown [66] that $\rho_S(T)$, defined as the fraction of the system that decouples from an externally induced rotation, is expressed by:

$$\rho_S(T) = \frac{4m^2T}{\hbar^2 I_c} \langle A^2 \rangle. \quad (1.36)$$

Here I_c is the classical moment of inertia of the cluster, and A the total area swept by the many-particle paths, projected onto a plane perpendicular to one of the three equivalent rotation axes. There have been several attempts to formulate an estimator for the *local* superfluid response to be used in QMC simulations, especially in the context of the study of doped helium clusters [23, 67, 68]. A proposed measure of the local superfluid response, frequently adopted in previous QMC calculations at finite temperature, is the radial density profile of particles involved in permutation cycles, sometimes with a lower cutoff (e.g., six particles)

for the length of the cycles considered. In a recent paper [42], Khairallah *et al.* utilized this measure to study the superfluid density of p -H₂ droplets. Because exchanges underlie SF, it is tempting to ascribe some quantitative value to the above-described measure; however, the theoretical shortcomings of such a local superfluid density estimator have been long recognized, specifically the fact that the area swept by the many-particle paths, whose square average is proportional to the total superfluid fraction, bears no direct relation to the number of particles involved in a permutation cycle [23].

Instead, in this work we computed profiles of radial superfluid density by means of a microscopic estimator recently proposed by Kwon *et al.* [68]; specifically, the local superfluid density $n_S(r)$ is given by:

$$\frac{n_S(r)}{n(r)} = \frac{4m^2 \langle AA(r) \rangle}{\beta \hbar^2 I_C(r)} \quad (1.37)$$

where $A(r)$ and $I_C(r)$ are, respectively, the contributions to A and I_C from a spherical shell of radius r centered at the center of mass of the cluster. The above estimator, contrary to the other proposed measures (which lack any theoretical foundation), is rigorously defined and integrates to the correct moment of inertia.

1.7.3 Evaluation of the statistical errors

We outlined in paragraph 1.4 how the thermal average of a physical observable \hat{O} can be estimated by means of an average of its values over a large set of many-particle paths \mathbf{X}_i ($i = 1, \dots, N_P$):

$$\langle O \rangle \approx \frac{1}{N_P} \sum_{i=1}^{N_P} O(\mathbf{X}_i). \quad (1.38)$$

Assuming the values $O(\mathbf{X}_i)$ independent and normally distributed, an estimate of the statistical uncertainty affecting the estimate of $\langle O \rangle$ is given by:

$$\sigma_{\langle O \rangle} \approx \sqrt{\frac{1}{(N_P - 1)} \sum_i^{N_P} (O(\mathbf{X}_i) - \langle O \rangle)^2}. \quad (1.39)$$

However, the configurations generated by the Metropolis algorithm are not independent, as they are generated through a random walk which clearly relates configurations visited sequentially. As a result, formula (1.39) underestimates the statistical error. To overcome this problem, one typically divides the set of configurations generated by means of the random walk in several *bins*, each including the same, relatively large number of *sequentially generated* configurations. For each bin, one can compute a *partial average* of the observable of interest, thereafter one performs the same statistical analysis described above, but on the reduced set of partial averages. Obviously, binning has no effect on the estimate of the average value, but affects that of the statistical uncertainty.

The procedure is as follows [69] (let us for simplicity assume that $N_P = 2^{\mathcal{L}}$, a condition that can always be fulfilled by discarding some of the initial configurations): one typically starts with a number of bins N_B equal to the number of configurations (i.e., each bin contains just one configuration). The zeroth estimate of the error, namely $\sigma_{\langle \hat{O} \rangle}^{(0)}$, is given by the specialization (with $j = 0$ and $N_B = N_P$) of the general formula:

$$\sigma_{\langle \hat{O} \rangle}^{(j)} \approx \frac{\sigma_B}{\sqrt{N_B}} = \sqrt{\frac{1}{N_B(N_B - 1)} \sum_{k=1}^{N_B} (\langle \hat{O} \rangle_k - \langle \hat{O} \rangle)^2}. \quad (1.40)$$

One then doubles the size of each bin (i.e., incorporating the estimates yielded by

two successively generated configurations), thereby reducing the number of bins by two, and computes a second estimate of the uncertainty (i.e., $\sigma_{\langle\hat{O}\rangle}^{(1)}$), based on the partial averages from each bin; the same procedure is iterated to obtain, using formula (1.40), $\mathcal{L} + 1$ estimates $\sigma^{(j)}$, $j = 0, 1, \dots, \mathcal{L}$. In the typical case, $\sigma^{(j)}$ will grow for small j , but then reach a plateau before j approaches \mathcal{L} too closely. If evidence of such a plateau is observed, then the convergence value can be taken as a reliable estimate of the statistical uncertainty on $\langle\hat{O}\rangle$. On the other hand, if no such plateau is seen then one can only conclude that the simulation did not take a sufficiently long time to provide a robust estimate of the statistical uncertainty of $\langle\hat{O}\rangle$.

Chapter 2

RESULTS

In this chapter we present our results for pure and isotopically doped molecular hydrogen clusters. Energetics, as well as structural and superfluid properties of p -H₂ and o -D₂ clusters are discussed in the next two sections, while the dependence of these properties on the isotopic composition of a mixed cluster in the third and fourth ones. Finally we discuss the relation between local and global superfluid response of p -H₂ clusters and test our theoretical predictions against different choices of the intermolecular potential.

2.1 p -H₂ clusters

2.1.1 Energetics

The total energy per p -H₂ molecule $e(N)$ as a function of the cluster size N , at $T=1$ K, computed using the Silvera-Goldman potential, is shown in Fig 2.1. Also shown in the figure are the estimates from Ref. [35]. For comparison purposes, we also show energies computed with the Buck potential; as we can see, binding

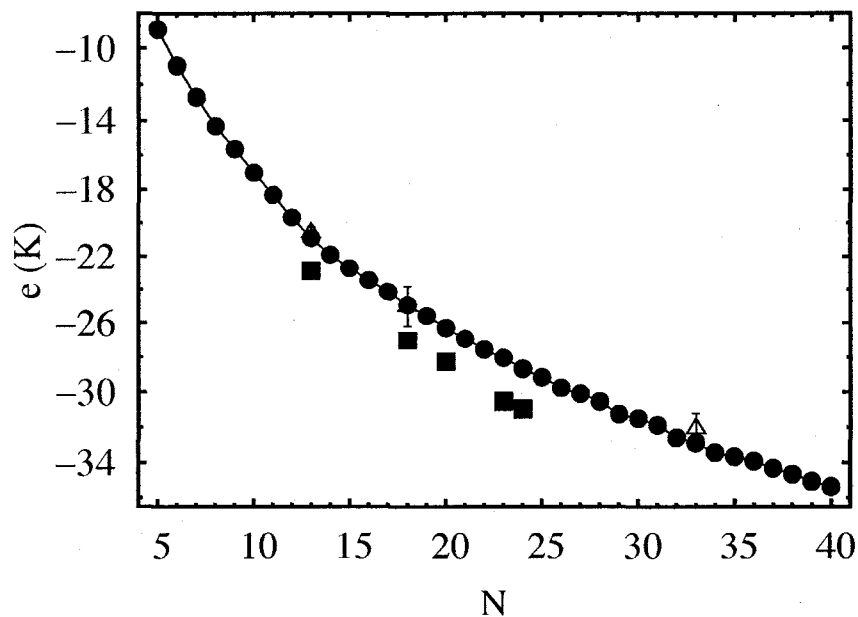


Figure 2.1: Energy per p -H₂ molecule versus cluster size N , at $T=1$ K. Estimates have been obtained using the SG (circles) and the Buck (boxes) potential. When not shown, statistical errors are of the order of, or smaller than the symbol size. Solid line is only a guide to the eye. Also shown for comparison are results from Ref. [35] (triangles).

energies estimated with the Buck potential are considerably greater than those computed with the SG interaction. For example, a cluster of 23 molecules is characterized by an energy some 2.5 K more negative than that obtained with the SG potential. Such a difference can be simply ascribed to the deeper attractive well (roughly 2 K at the minimum) of the Buck potential. We come back to a more detailed comparison of energies computed with different interactions, including the LJ potential, later on.

The energy per p -H₂ molecule is a monotonically decreasing function of the cluster size; the simple formula

$$e(N) = A_V + A_S N^{-\frac{1}{3}} + A_C N^{-\frac{2}{3}} \quad (2.1)$$

where A_V , A_S and A_C are volume, surface and curvature terms, fails to yield a reasonable fit to our data, as well as an accurate extrapolation of the bulk energy (~ -90 K) [55], to indicate that the physics of the bulk is not yet approached by clusters of size studied here. This should be compared with the case of small ⁴He clusters (of size up to $N=50$), for which the same formula provides an acceptable fit to the data, even though the extrapolated bulk energy differs from the actual value by 7% [70].

The energy values shown in Fig. 2.1 for the Buck potential are generally consistent with those obtained by Guardiola and Navarro [51], who computed them at $T=0$ by means of Diffusion Monte Carlo simulations. We have computed energetics for several clusters at T lower than 1 K, and estimate the maximum difference between our results at $T=1$ K and those extrapolated to $T=0$ to be less than 0.3 K. However, for some clusters our energies are significantly lower than those of Ref. [51]. We note, indeed, that our data for the Buck potential are in agreement with those computed by the same authors in a more recent work [52] and by other groups, using $T=0$ QMC methods [50, 71].

Because in the case of helium the equilibrium condensed phase is liquid, no qualitative structural change occurs as the size of the cluster is increased. For hydrogen, on the other hand, since the equilibrium bulk phase at $T=0$ is solid, the

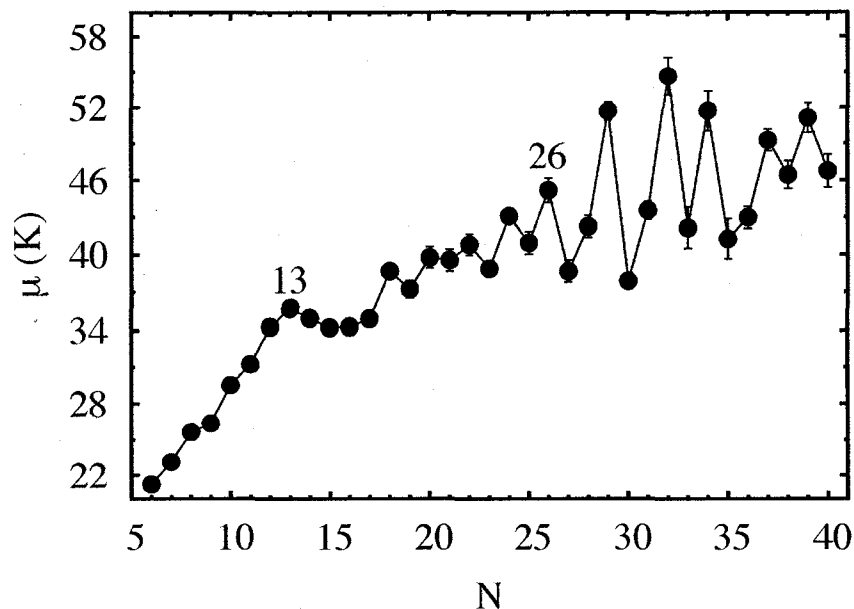


Figure 2.2: Chemical potential of p -H₂ clusters versus cluster size N . Estimates have been obtained using the SG potential. When not shown, statistical errors are of the order of, or smaller than the symbol size. Solid line is only a guide to the eye. Numbers refer to stable (“magic”) clusters.

structure must evolve from liquid- to solid-like¹, presumably in a non-monotonic fashion, going through structures of different shapes and geometries. It is therefore scarcely surprising that a simple formula like (2.1) should not offer equally acceptable a fit as for helium clusters. Recent $T=0$ QMC calculations [50, 51] have pointed out the existence of magic sizes (i.e., $N=13$) corresponding to particularly stable clusters. In order to have a clear visual identification of these magic

¹Obviously, because a cluster is a finite system one cannot speak rigorously of “solid” and “liquid”. Nevertheless, we shall use this loose, but intuitive terminology for the sake of clarity.

sizes, we plot in Fig. 2.2 the chemical potential μ as a function of the cluster size defined as:

$$\mu(N) = E(N - 1) - E(N) \quad (2.2)$$

where $E(N)$ is the total energy of a cluster of N molecules. The chemical potential increases monotonically for $N \leq 13$; for clusters of greater size, its behavior is rather irregular. Local maxima are observed for particular values of N (i.e., $N=13$ and 26). The corresponding clusters are characterized by considerable stability, and rather compact structure.

In the following we show that $p\text{-H}_2$ clusters of size $N < 22$ display properties consistent with a liquid-like superfluid character; the stability of $(p\text{-H}_2)_{13}$ is, in our view, not the sign of the occurrence of a particular solid-like structure, as proposed in Ref. [51], but rather of first-shell completion (which does not rule out liquid-like behavior) [31, 34].

2.1.2 Superfluidity

Data for the superfluid fraction $\rho_S(T)$ of $(p\text{-H}_2)_{18}$ are shown in Fig 2.3. As expected, $\rho_S(T)$ is a monotonic decreasing function of T ; this cluster is essentially entirely superfluid (i.e., $\rho_S(T) \simeq 1$) at $T \leq 1$ K. Then, $\rho_S(T)$ drops to a value ~ 0.27 in a temperature interval of 1.5 K and decreases more slowly at higher T .

A finite system cannot undergo a phase transition in a strict sense; therefore, in order to assign a “transition temperature”, one must resort to some arbitrary criterion. Because the notion of superfluid fraction is scarcely meaningful when the average number of molecules in the superfluid phase is ~ 1 , we empirically define our “transition temperature” T_c as that at which $N\rho_S(T_c) \simeq 2$. Hence the

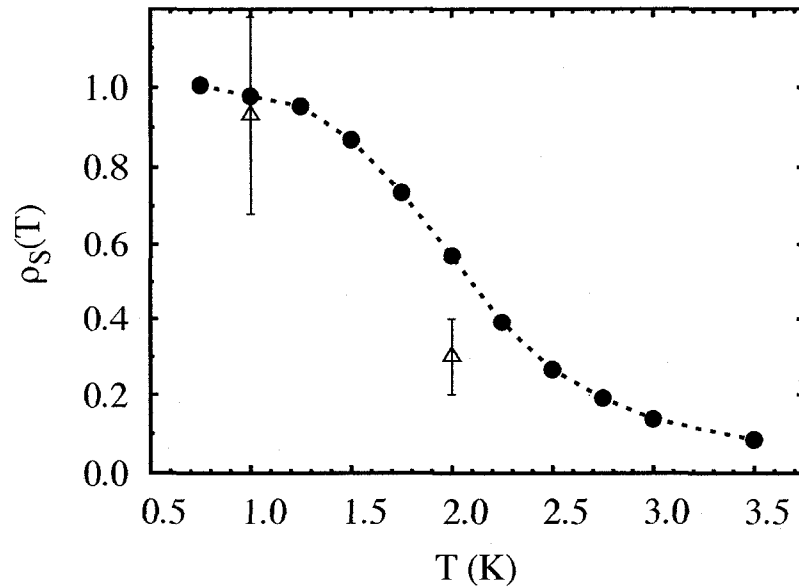


Figure 2.3: Temperature dependence of the superfluid fraction $\rho_S(T)$ for a cluster of 18 p -H₂ molecules (circles). Estimates are obtained with the SG potential. Dotted line is only a guide to the eye. When not shown, statistical errors are smaller than the symbol size. Also shown for comparison are results from Ref. [35] (triangles).

estimated transition temperature is $T_c \approx 3$ K.

The superfluid fraction computed with the SG potential (circles) as a function of the cluster size at $T=1$ K is presented in Fig 2.4. Clusters of size $N < 22$ are entirely superfluid (or nearly so, at least within the precision of our calculations), and display a temperature dependence of the superfluid fraction similar to that shown in Fig. 2.3 for $N=18$.

An interesting, non-monotonic trend is observed (Fig. 2.4) for the superfluid

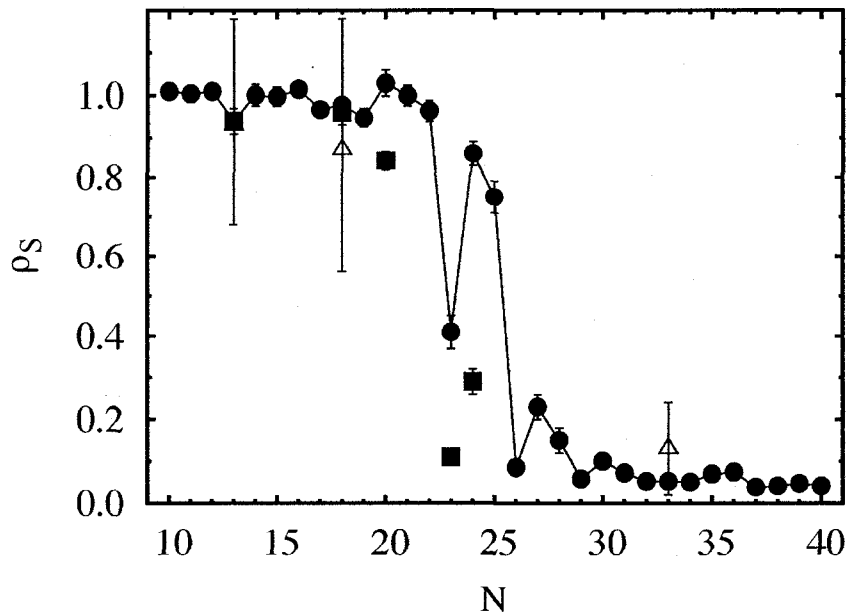


Figure 2.4: Superfluid fraction of p -H₂ clusters versus cluster size N , at $T=1$ K. Estimates have been obtained using the SG (circles) and the Buck (boxes) potential. When not shown, statistical errors are of the order of, or smaller than the symbol size. Solid line is only a guide to the eye. Also shown for comparison are results from Ref. [35] (triangles).

fraction at low T of clusters of $N \geq 22$ molecules. The value of $\rho_S(T=1$ K), is close to unity for $N=22$, and drops to a local minimum if a single molecule is added (i.e., for $N=23$). It then rises again to approximately 85%, if another molecule is added ($N=24$), and remains relatively large for $N=25$. The addition of another molecule, from $N=25$ to $N=26$, again causes an abrupt drop of ρ_S , to less than 0.1. On adding one more molecule, ρ_S becomes again significant (approximately 25%), but drops sharply once more at $N=29$; it remains small, while still featuring

noticeable oscillations, for greater N values.

Generally speaking, as the number N of particles increases, the physics of a cluster ought to approach that of the bulk; in its bulk phase at low T , p -H₂ is an insulating (non-superfluid) crystal, i.e., its character is completely different from that of small clusters (i.e., $N < 22$), which remain liquid-like and are entirely superfluid. Data in Fig. 2.4 show that the evolution from liquid- to solid-like does not occur continuously, i.e., bulk properties do not gradually emerge when N increases.

In particular, we interpret the peculiar behavior of ρ_S observed for $N \geq 22$, as due to alternating superfluid (liquid-like) or insulating (solid-like) character of the clusters. It seems plausible that drastic changes of the superfluid fraction, occurring upon adding just one molecule, ought to be directly connected with structural changes.

In order to illustrate this point, we show in Fig. 2.5 profiles of radial density $[n(r)]$, computed with respect to the center of mass of the cluster, at $T=1$ K. For $N=15$, the large value of $n(r \rightarrow 0)$ and the local minimum for $r \approx 2 \text{ \AA}$ indicate the presence of a single p -H₂ molecule in the center of the cluster. Other molecules form a floppy shell around the central one, as shown by the peak at $r=4 \text{ \AA}$. On increasing the cluster size, qualitative changes occur at $N \sim 22$. The value of $n(r \rightarrow 0)$ becomes negligible, i.e., the center of the cluster is no longer occupied by a molecule. There is a peak at about 2 \AA from the center, as an inner molecular shell forms. A second, broader peak at larger distance ($r \approx 5 \text{ \AA}$) corresponds to the formation of an outer shell.

The main structural change, going from $N=25$ to $N=26$, is that the first peak becomes significantly sharper, and its height increases by some 40% (see Fig. 2.5).

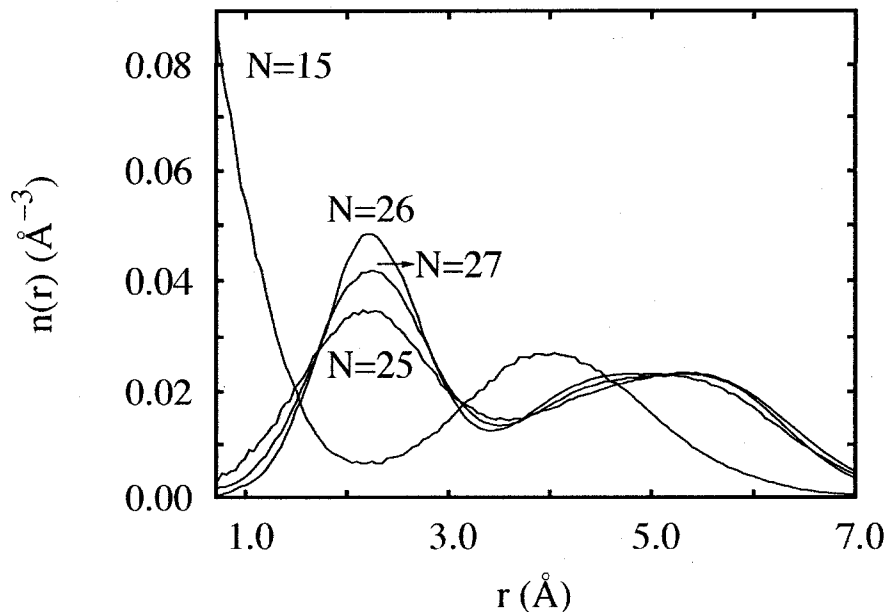


Figure 2.5: Radial density, at $T=1$ K, computed with respect to the center of mass, for clusters with 15, 25, 26, and 27 p -H₂ molecules. Estimates have been obtained using the SG potential. Statistical errors, not shown for clarity, are of the order of $5 \times 10^{-4} \text{ \AA}^{-3}$ or less.

We interpret this as evidence that the inner shell as well as the entire cluster becomes more solid-like, with molecules localized and quantum exchanges suppressed, both in the first shell as well as between the first and second shells. If another molecule is added, the density profile for $N=27$ features a first-shell peak and an intershell minimum of heights intermediate between those of the $N=25$ and $N=26$ cases, and ρ_S increases to a value much lower than that for $N=25$, but significantly greater than that for $N=26$. Thus, the addition of a molecule to the $N=26$ has the effect of frustrating the solid order of the inner shell, increasing

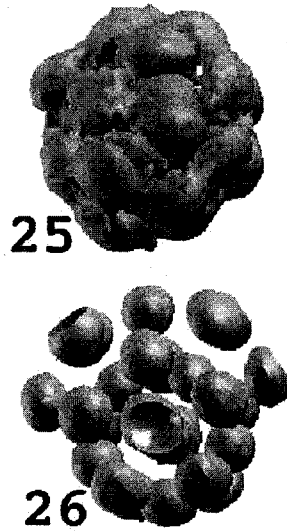


Figure 2.6: Three dimensional representation of a cluster comprising 25 and 26 $p\text{-H}_2$ molecules (interacting via the SG potential) at a temperature of 1 K. Even though the information provided by this kind of figure is purely qualitative, the structural difference is evident: $(p\text{-H}_2)_{25}$ is essentially liquid-like (molecules are highly delocalized), while $(p\text{-H}_2)_{26}$ is solid-like (molecules are more localized and clearly distinguishable).

molecule delocalization and leading to quantum exchanges.

Particularly telling is the graphical representation of the three-dimensional structure of the clusters $(p\text{-H}_2)_{25}$ and $(p\text{-H}_2)_{26}$ at $T=1$ K shown in Fig. 2.6; these figures are produced as explained in Ref. [31]. The solid-like properties of the cluster $(p\text{-H}_2)_{26}$ are evident. Its structure consists of three rings of five molecules, with four other molecules linearly arranged along the axes of the rings, while the remaining seven molecules form an outer shell. Although their position is smeared out by zero-point fluctuations, the various molecules in the cluster can be clearly identified, indicating that they enjoy a fairly high degree of spatial localization; consequently, exchanges among different molecules are highly suppressed (though not completely absent, as shown in Fig. 2.7), and the superfluid response is weak.

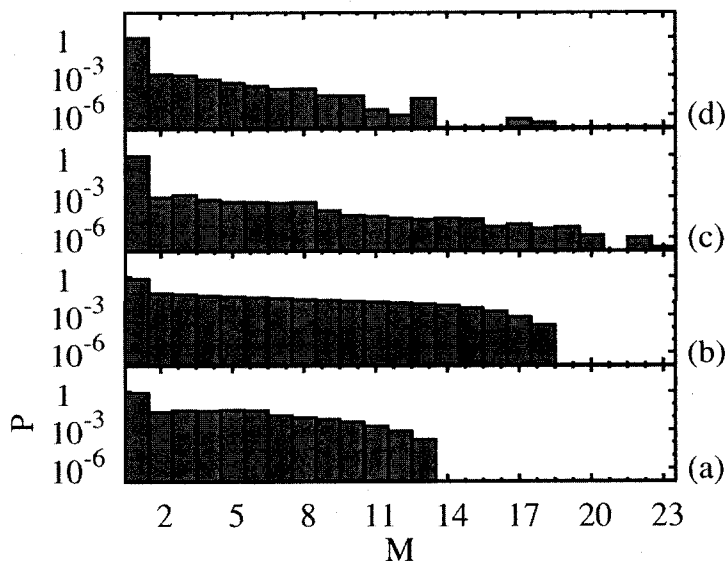


Figure 2.7: Statistics of permutation cycles involving $1 \leq M \leq N$ molecules for the clusters $(p\text{-H}_2)_{13}$ (a), $(p\text{-H}_2)_{18}$ (b), $(p\text{-H}_2)_{26}$ (c) and $(p\text{-H}_2)_{33}$ (d) at $T=1$ K. SG potential has been used.

Conversely, the equilibrium positions of molecules in the cluster $(p\text{-H}_2)_{25}$ cannot be clearly identified, and the entire system appears amorphous. Because of their pronounced delocalization, molecules have a strong propensity to be involved in quantum exchanges, hence the large superfluid response observed. The physics is reminiscent of that of the insulating-superfluid quantum phase transition observed in lattice models of hard core bosons, where a superfluid, non-crystalline phase appears as the system is driven away from commensuration (where it is an insulator) [72]. Fig. 2.7 shows the statistics of exchange cycles involving $1 \leq M \leq N$ molecules for the clusters (from bottom to top) $(p\text{-H}_2)_{13}$, $(p\text{-H}_2)_{18}$, $(p\text{-H}_2)_{26}$ and $(p\text{-H}_2)_{33}$ at a temperature $T=1$ K. Long exchange cycles are known to underlie su-

perfluidity. The value of the superfluid fraction of the smaller clusters (i.e., $N=13$ and 18) is close to 1, and exchanges occur involving up to N molecules, with significant frequency. On the other hand, in the case of $(p\text{-H}_2)_{26}$ and $(p\text{-H}_2)_{33}$ ρ_S is less than 0.1; remarkably, however, exchange cycles involving as many as 23 and 18 molecules respectively have finite, albeit small, statistical weight. This observation is consistent with that made in Ref. [73] (based on a PIMC simulation which did not explicitly include exchanges).

The superfluid fraction computed with the Buck potential (boxes in Fig. 2.4) is in excellent agreement with that obtained with the SG, for those clusters that are liquid-like (i.e., with $N \leq 22$). Quantitative differences (i.e., lower values of ρ_S obtained with the Buck potential, as shown in Fig. 2.4) occur for bigger clusters (which generally display more solid-like behavior), due to the more attractive character of the Buck potential, which results in greater molecular localization. However, the observed trend is qualitatively identical (for details see section 2.6)

2.1.3 Quantum melting

Some clusters of size $N > 22$, feature a fascinating behavior in the temperature range explored in this work; we discuss in detail the case of $(p\text{-H}_2)_{23}$, for which the superfluid fraction takes a local minimum. Fig. 2.8 shows the values of the superfluid fraction and of the potential energy per molecule, recorded during a typical Monte Carlo run for a cluster of 23 $p\text{-H}_2$ molecules at $T=1.4$ K and $T=1$ K. In particular, we show consecutive block averages of ρ_S and V , each block consisting of 500 sweeps (a sweep is a sampling cycle which starts with the opening and ends with the closing of the worm [37, 38]).

Despite the large fluctuations affecting the values of ρ_S , two different regimes

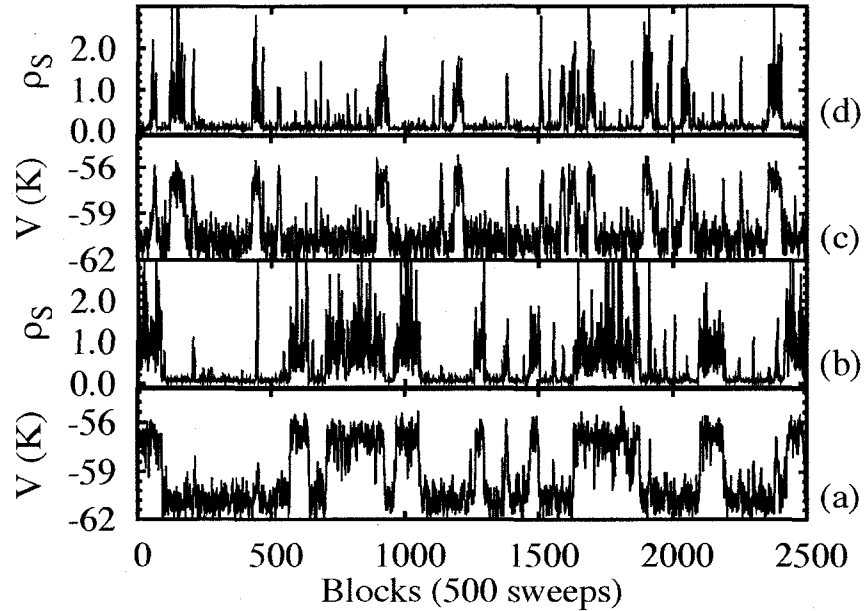


Figure 2.8: Potential energy per molecule and superfluid fraction observed during a typical Monte Carlo run (see text) for a cluster of $N=23$ $p\text{-H}_2$ molecules at $T=1$ K (panels a and b) and $T=1.4$ K (panels c and d). Estimates have been obtained using the SG potential. The coexistence of two phases can be easily recognized since the averages of ρ_S and V simultaneously switch between high (liquid-like superfluid phase) and low (solid-like insulating phase) values. The liquid-like superfluid phase becomes dominant as T is lowered.

can be easily identified: one in which the superfluid fraction is high, with an average value close to 1, and the other characterized by low values of ρ_S , with an average value close to zero. The potential energy, correspondingly, takes on high (low) values when ρ_S is large (small). While the behavior of the superfluid fraction is consistent with coexistence of two phases, characterized by large and small superfluid response, the information given by the potential energy suggests that these two phases have also liquid-like and solid-like properties. For, the switching of the

average value of the potential energy between two different regimes, separated by some ~ 6 K, can be interpreted as due to the system visiting relatively ordered, solid-like, insulating configurations (characterized by low potential energy), and disordered, liquid-like, superfluid ones. The coexistence between two distinct (disordered and ordered) phases is consistent with the observation made in Ref. [74] for classical clusters.

On decreasing the temperature from $T=1.4$ K (panels *c* and *d* of Fig. 2.8) to $T=1$ K (panels *a* and *b* of the same figure), the superfluid (liquid-like) phase (i.e., large values of ρ_S and V) is observed during a greater fraction of the simulation time, and becomes dominant as T approaches 0 K; the cluster therefore “melts” at low T . This process is ostensibly induced by zero-point motion, and the ensuing exchanges of molecules, whose importance increases as T is lowered. In this sense, one could state that melting is driven by Bose statistics, i.e., it is associated to the energy contribution due to quantum exchanges.

On the other hand, when T is sufficiently high, quantum exchanges are suppressed and the system “freezes” in a solid-like structure. Other clusters of size $N > 22$ presumably display the same physics, albeit at lower T . For example evidence of *quantum melting* has also been found for $(p\text{-H}_2)_{27}$ at $T \sim 0.5$ K and for $(p\text{-H}_2)_{26}$ at $T \sim 0.1$ K. It has to be mentioned that at the remarkably low temperature of 0.0625 K even the cluster $(p\text{-H}_2)_{48}$, the largest studied in this work displays remarkable superfluid properties. It is important to stress that the behavior illustrated in Fig. 2.8 is different from that of a cluster that is liquid-like, and simply not 100% superfluid; indeed, in such a case superfluid fraction and potential energy fluctuate around their average values, with no evidence of the switching displayed in Fig. 2.8. This is precisely what we find for clusters of size $N < 22$, which are

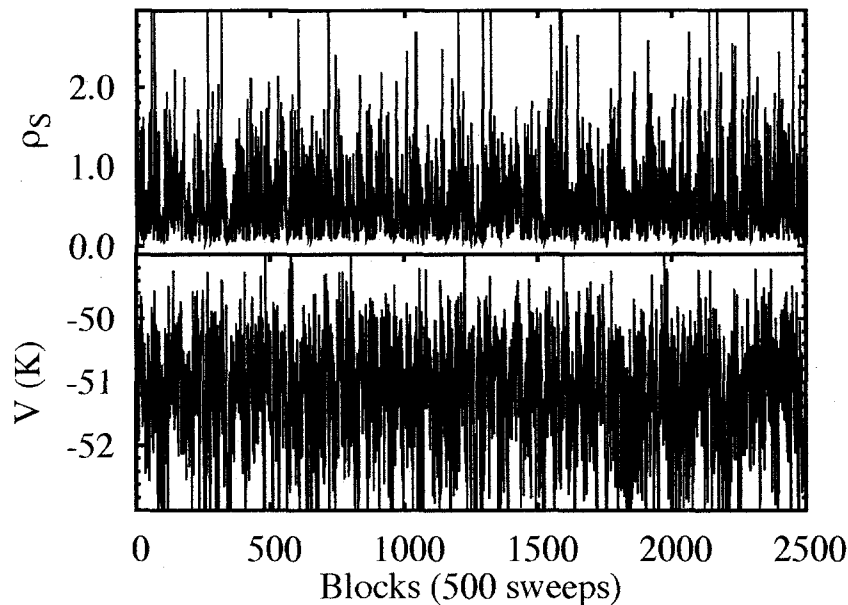


Figure 2.9: Potential energy per molecule and superfluid fraction recorded during a typical Monte Carlo run for a cluster of $N=18$ p -H₂ molecules at $T=2$ K. Estimates are obtained with the SG potential. In this case, ρ_S and V simply oscillate around their average values (approximately 0.6 for ρ_S) without featuring the clear, simultaneous “jumps” observed in Fig 2.8. This system is found to be liquid-like in the range of temperature considered in this work.

liquid-like at all temperatures, with superfluid (normal) component growing at low (high) T (see Fig. 2.9).

Our interpretation is supported by the evolution with T of the radial density profiles $n(r)$ of the cluster, defined with respect to its center of mass. In Fig. 2.10, radial density profiles for $(p\text{-H}_2)_{23}$ and $(p\text{-H}_2)_{18}$ at $T=0.75$ K (diamonds and boxes) as well as at $T=2$ K (stars and triangles) are shown. A cluster comprising 23 p -H₂ molecules at a temperature $T=2$ K, displays a two-shell structure with one

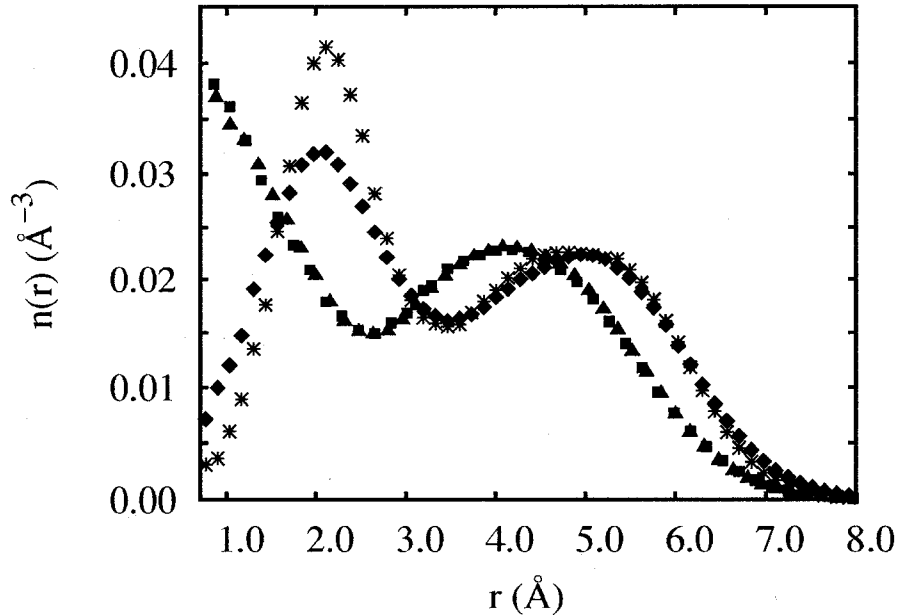


Figure 2.10: Radial density profiles for a $p\text{-H}_2$ cluster with $N=18$ [$T=0.75$ K (boxes) and $T=2$ K (triangles)] and $N=23$ [$T=0.75$ K (diamonds) and $T=2$ K (stars)] $p\text{-H}_2$ molecules. Estimates have been obtained with the SG potential. Statistical errors, not shown for clarity, are of the order of $5 \times 10^{-4} \text{ \AA}^{-3}$ or less.

sharp peak at $r \approx 2 \text{ \AA}$, and a second broader one at about 5.5 \AA . As T is lowered to 0.75 K , the first peak becomes significantly broader, and its height decreases. Therefore, molecules in the inner shell are less localized, and the cluster is more liquid-like, with greater propensity for quantum exchanges both in the first shell, as well as between the first and the second shells. For a cluster of 18 molecules, on the other hand, density profiles stay the same, as T is lowered from 2 K to 0.75 K , featuring one particle at the center of mass [signaled by the large value of $n(r \rightarrow 0)$] and an outer shell, separated by a shallow minimum (indicative of liquid-

like structure). The value of the superfluid fraction of $(p\text{-H}_2)_{18}$ increases from about 0.57 to roughly 1 when T goes from 2 K to 0.75 K; however, this change is hardly reflected in the cluster structure. Quite differently, the increase of ρ_S in a cluster of 23 molecule, observed in the same temperature range, reflects a substantial change in the structure, due to quantum melting (as shown in Fig. 2.10). This phenomenon clearly exemplifies the importance of quantum effects on the structural properties of small systems, which has been also investigated in clusters of neon, which display moderate quantum character [75, 76, 77].

We conclude by stressing once again that, even though the results presented in this section are obtained using the SG potential, similar physics is observed if the more attractive Buck potential is adopted. The only quantitative changes are the values of the superfluid fraction, which are generally lower than those computed with the SG interaction for a given T . However, quantum melting is observed in clusters of the same size, even if the potential due to Buck is used, i.e., it is broadly independent of the details of the interaction (see paragraph 2.6).

2.2 $o\text{-D}_2$ clusters

Next, we discuss the properties of $o\text{-D}_2$ clusters; here too, we regard $o\text{-D}_2$ molecules as bosons of spin zero [78], with a mass twice that of $p\text{-H}_2$ molecules. We computed (with the SG potential) energy, superfluid fraction and radial density profiles for clusters of size N ranging from 3 to 20 molecules at $0.5 \text{ K} \leq T \leq 2.0 \text{ K}$.

2.2.1 Energetics

The total energy per o -D₂ molecule as a function of the cluster size, at $T=0.5$ K is shown in Fig. 2.11.

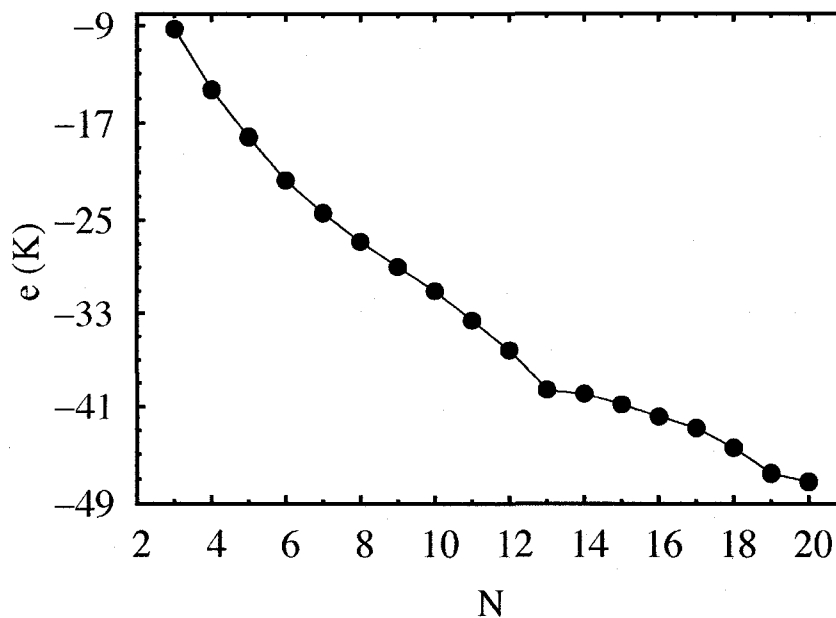


Figure 2.11: Energy per o -D₂ molecules e versus cluster size N at a temperature of 0.5 K. Statistical errors are smaller than the symbol size. Solid line is only a guide to the eye.

For $N=3$, the energy has a value close to -9 K, which smoothly decreases with N , reaching a value of roughly -36 K for $N=12$. On adding one more molecule, the energy drops to about -39.5 K ($N=13$), and decreases more slowly for N up to 17. For greater values of N an important drop of the energy is still observed at $N=19$.

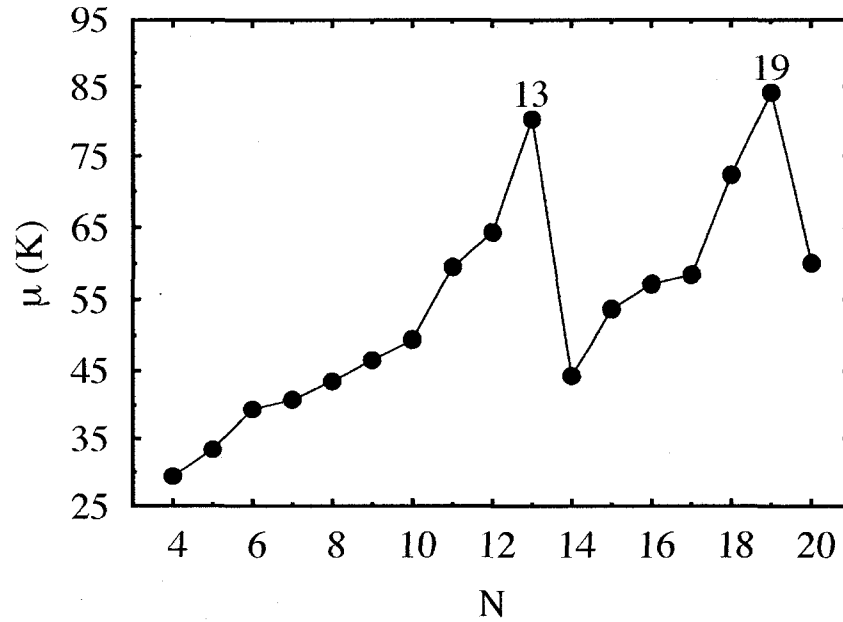


Figure 2.12: Chemical potential of o -D₂ clusters versus cluster size N . When not shown, statistical errors are of the order of, or smaller than the symbol size. Solid line is only a guide to the eye. Numbers refer to stable (“magic”) clusters.

As in the previously discussed case of p -H₂ clusters, a fit of our data using Eq. 2.1 is difficult, and does not allow an accurate estimate of the bulk energy; moreover, the chemical potential (see Fig. 2.12), displaying sharp local maxima for $N=13$ and 19 confirms the existence of “magic” sizes, corresponding to highly stable clusters [i.e., $(o\text{-D}_2)_{13}$ and $(o\text{-D}_2)_{19}$].

2.2.2 Superfluidity

Fig. 2.13 shows $\rho_S(T)$ for a cluster consisting of 11 o -D₂ molecules. The mono-

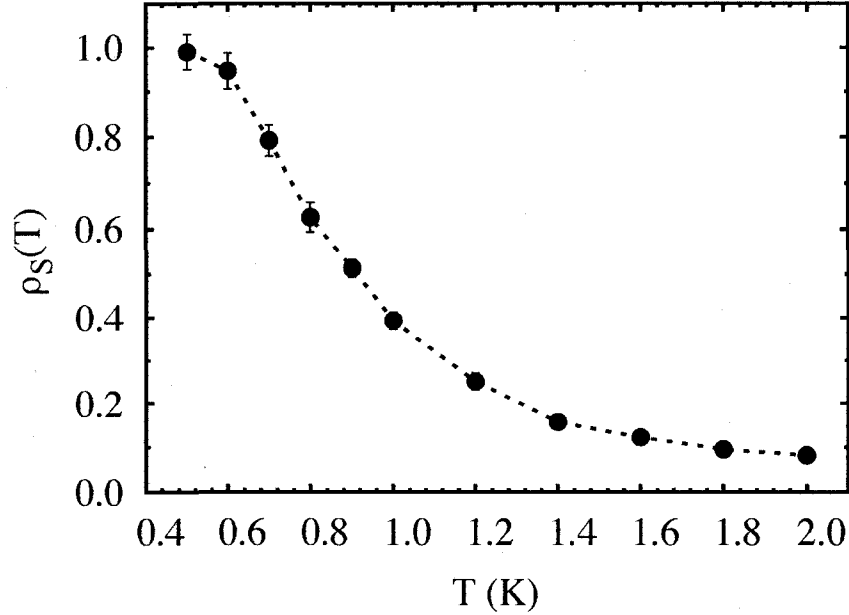


Figure 2.13: Temperature dependence of the superfluid fraction $\rho_S(T)$ for a clusters of 11 $o\text{-D}_2$ molecules. Dotted line is only a guide to the eye. When not shown, statistical errors are smaller than the symbol size.

tonically decreasing trend is qualitatively similar to that in Fig. 2.3 for $(p\text{-H}_2)_{18}$. However, the superfluid fraction of the cluster $(o\text{-D}_2)_{11}$ decreases more rapidly with T . In particular, it is approximately 1 at $T \leq 0.5$ K, and suddenly drops to a value $\simeq 0.39$ (corresponding to roughly 4 molecules in the superfluid phase) when T increases by 0.5 K. At higher temperature, the superfluid fraction becomes essentially zero (in the sense explained in the previous section) for $T \simeq 1.4$ K, at which the average number of molecules in the superfluid phase is less than two. It is important to note that, while the cluster $(p\text{-H}_2)_{18}$ is almost 60% su-

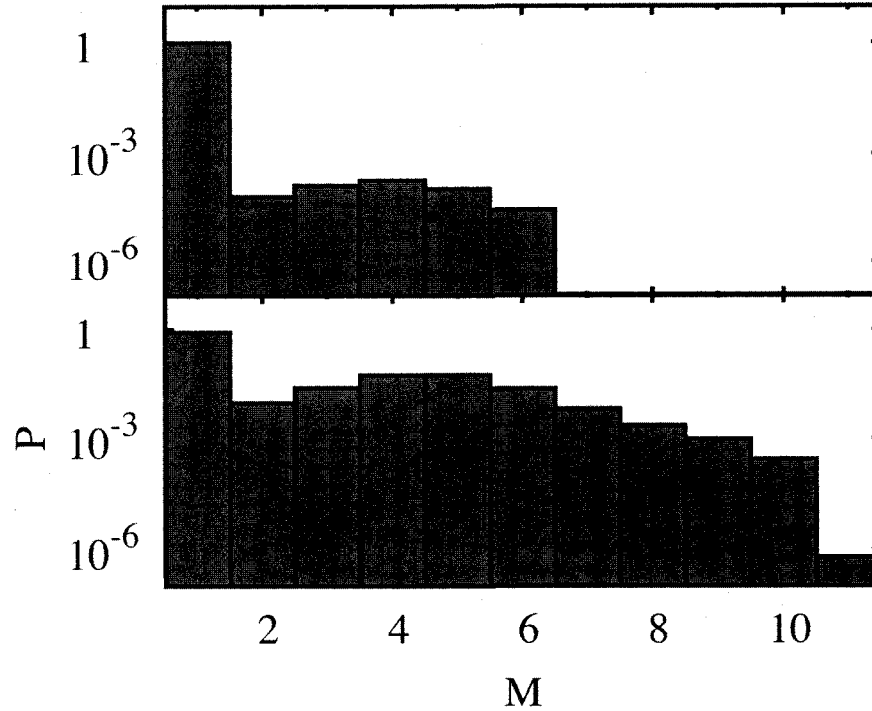


Figure 2.14: Statistics of permutation cycles involving $1 \leq M \leq N$ molecules for the cluster $(o\text{-D}_2)_{11}$ at $T=0.5$ K (lower panel) and $T=2$ K (upper panel).

perfluid at $T=2$ K (Fig. 2.3), $(o\text{-D}_2)_{11}$ at the same temperature is non-superfluid, and the probability of observing permutation cycles comprising more than 3 $o\text{-D}_2$ molecules is less than 5×10^{-4} . The statistics of many-particle permutations in the system $(o\text{-D}_2)_{11}$ at $T=0.5$ K (lower panel) and 2 K (upper panel) shown in Fig. 2.14 points out how, at high T , long exchange cycles disappear, as clusters behave more classically.

The size dependence of the superfluid fraction at two different temperatures

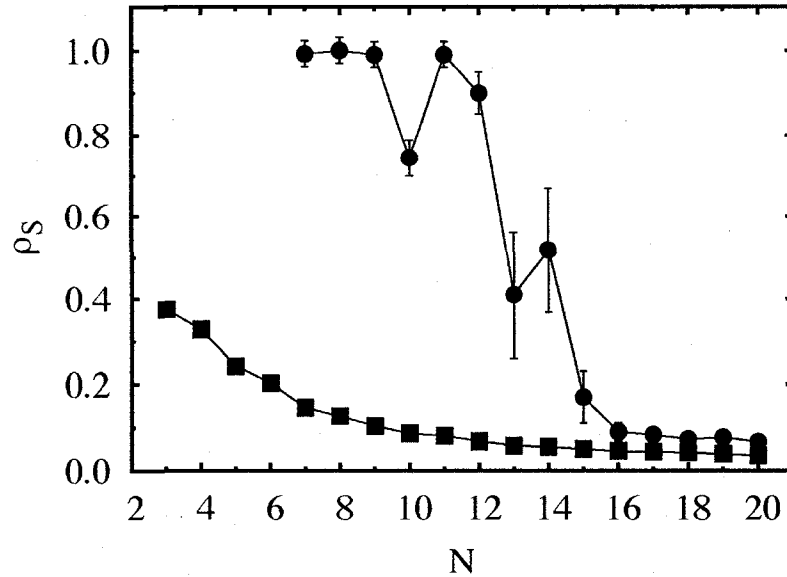


Figure 2.15: Superfluid fraction of o -D₂ clusters versus cluster size N , at $T=0.5$ K (circles) and $T=2$ K (boxes). When not shown, statistical errors are of the order of, or smaller than the symbol size. Solid lines are only guides to the eye.

($T=0.5$ and 2 K) is shown in Fig. 2.15. At $T=0.5$ K, small o -D₂ clusters ($N \leq 9$) are entirely superfluid, while for larger values of N the trend of ρ_S is consistent with a noticeable dependence on the cluster size, similarly to what was observed for p -H₂ clusters with $N \geq 22$. A local minimum is observed for $N=10$; then the superfluid fraction grows to a value close to 1 for $N=11$, and remains relatively large at $N=12$.

Large fluctuations, observed during lengthy simulations, render the determination of the value of ρ_S quite difficult for clusters greater than 11 o -D₂ molecules. Nevertheless, we can conclude from our data that clusters of up to 14 molecules still

feature a significant superfluid response, which instead is close to zero for larger clusters. As expected, at higher temperatures ρ_S becomes progressively smaller and many-particle permutation cycles are almost absent.

The behavior shown in Fig. 2.8, indicative of quantum melting, has been observed for large o -D₂ clusters at much lower temperature. For example the cluster $(o\text{-D}_2)_{26}$ has been found to melt at a temperature as low as $T = 0.0625$ K.

2.2.3 Structure

Radial density profiles of the clusters $(o\text{-D}_2)_7$, $(o\text{-D}_2)_{10}$ and $(o\text{-D}_2)_{11}$ at $T=0.5$ K are shown in Fig. 2.16. The cluster $(o\text{-D}_2)_7$ features a single-shell structure, with a broad peak at about 2.5 Å, consistent with a high degree of delocalization of the molecules. For $N=10$, the probability of having the center of the system occupied by a molecule becomes significant, and the peak is shifted to higher distances by roughly 1 Å. The shallow minimum, which appears at $r \simeq 2$ Å, suggests that exchanges are frequent, and not restricted to molecules in the first shell, i.e., they involve also the molecule in the center of the cluster. Important structural differences characterize $(o\text{-D}_2)_{11}$; as shown by the small value of the radial density at the minimum, and by the increased height of the first peak in Fig. 2.16, the molecule in the center of the cluster is strongly localized [see also the high value of $n(r \rightarrow 0)$], and scarcely participates in multi-particle exchanges. Remarkably, the superfluid fraction of all these systems is large, close to 1 for $N=7$ and 11. The inset of Fig. 2.16 compares radial density profiles of $(o\text{-D}_2)_{13}$ and $(p\text{-H}_2)_{13}$ at $T=0.5$ K; the effect of the mass difference on the structural properties is evident. Indeed, the density profile of $(p\text{-H}_2)_{13}$ reflects the liquid-like nature of such a system, whereas in the case of $(o\text{-D}_2)_{13}$, structural details (i.e., pronounced

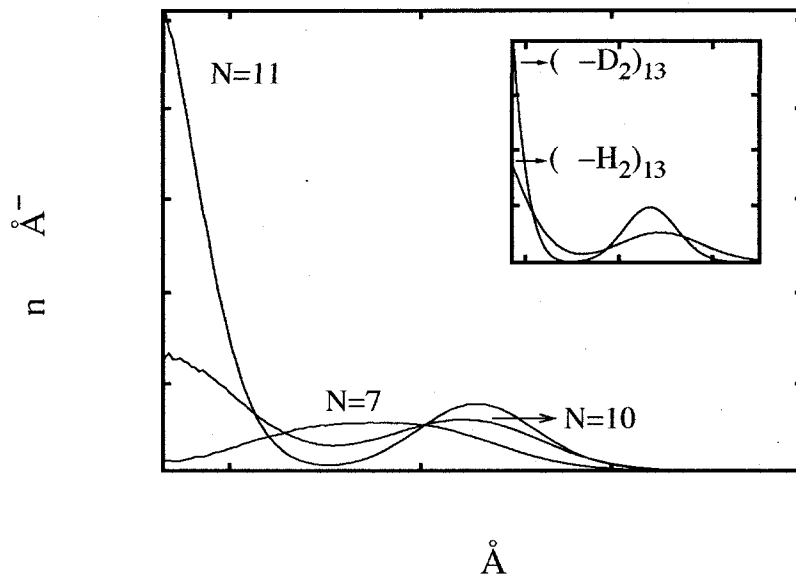


Figure 2.16: Radial density profiles for o -D₂ clusters with $N=7$, 10 and 11, at $T=0.5$ K. The inset shows the radial density profiles of $(o\text{-D}_2)_{13}$ and $(p\text{-H}_2)_{13}$ at the same temperature. Statistical errors, omitted for clarity, are of the order of $5 \times 10^{-4} \text{ \AA}^{-3}$ or less.

first-shell peak and the small value of the radial density at the minimum) are consistent with a more orderly (i.e., solid-like) structure.

It has been already pointed out how local maxima of the chemical potential correspond to magic clusters, featuring greater stability than others (see Fig. 2.12). Here, we discuss in detail the case of $(o\text{-D}_2)_{19}$. In Fig. 2.17 we show the three-dimensional structure of clusters comprising $N=18$ and 19 $o\text{-D}_2$ molecules, at $T=0.5$ K. The cluster $(o\text{-D}_2)_{18}$ is made of three rings of five molecules, with the remaining three molecules linearly arranged along the axes of the rings. On adding a single molecule ($N=19$), which also positions itself along the axes of the rings, the

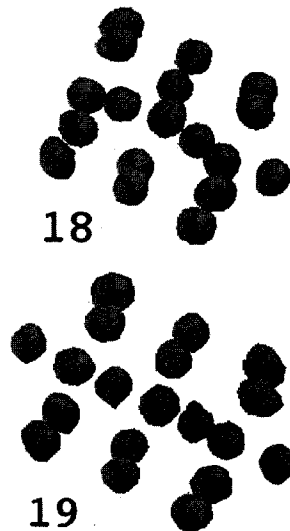


Figure 2.17: Three-dimensional representation of clusters comprising 18 and 19 o -D₂ molecules, at $T=0.5$ K. Both systems have solid-like properties, as molecules enjoy a high degree of localization. However, $(o\text{-D}_2)_{19}$ features greater stability, due to its more symmetric structure (see text).

structure becomes symmetric with respect to the plane of the central ring. Since both $(o\text{-D}_2)_{18}$ and $(o\text{-D}_2)_{19}$ at $T=0.5$ K are solid-like and insulating (i.e., molecules are clearly distinguishable and the value of ρ_S is less than 0.1), the sharp maximum of the chemical potential at $N=19$ appears not to be related to noticeable structural changes (i.e., from more liquid- to solid-like, as observed, at $T=1$ K for $p\text{-H}_2$ when N increases from 25 to 26²), but rather to the pronounced symmetry of this cluster.

²Recent $T=0$ QMC calculations found no evidence of the magic cluster $(p\text{-H}_2)_{26}$ [52, 79]. This is consistent with the fact that no shell completion occurs at $N=26$ and with the quantum melting of this cluster (for details see section 2.5).

2.3 Isotopically doped p -H₂ clusters

In this section, we present results of a microscopic study of p -H₂ clusters doped with isotopic impurities; specifically, we investigate the effect of the substitution of few p -H₂ with o -D₂ (or, o -H₂) molecules, in $(p\text{-H}_2)_N$ clusters that are entirely (or, almost entirely) superfluid. As discussed previously (see sections 2.1 and 2.2), due to the different mass of their constituents, p -H₂ and o -D₂ clusters display different superfluid response. For example a cluster comprising 20 p -H₂ molecules at $T=0.5$ K is liquid-like and superfluid, while at the same temperature a cluster comprising the same number of o -D₂ molecules is solid-like and insulating. Therefore the study of isotopically doped p -H₂ clusters comprising a total of about 20 molecules can provide important information on how solid-like properties emerge in a liquid-like p -H₂ cluster when p -H₂ molecules are progressively substituted with o -D₂ ones.

For definiteness, we focus on clusters of size $N \geq 16$, at the two temperatures $T=0.5$ and 1 K. The model adopted is the usual, namely the system is regarded as a collection of N_H p -H₂ and $N_D = N - N_H$ o -D₂ (o -H₂) molecules regarded as Bose particles of spin $S=0$ ($S=1$) and interacting via the SG pair potential.

Fig. 2.18 shows the superfluid fraction ρ_{SH} of the p -H₂ component of an isotopically doped p -H₂ cluster, as a function of the cluster size N at $T=1$ K (lower panel) and $T=0.5$ K (upper panel). Different symbols refer to a different number of substitutional o -D₂ or o -H₂ molecules (see figure caption). When a single p -H₂ molecule is replaced by an o -D₂ one, ρ_{SH} is relatively little affected for $N < 22$, with respect to a pristine p -H₂ cluster, but is suppressed substantially in larger clusters, particularly at higher T . For example, the substitution of one o -D₂ in a

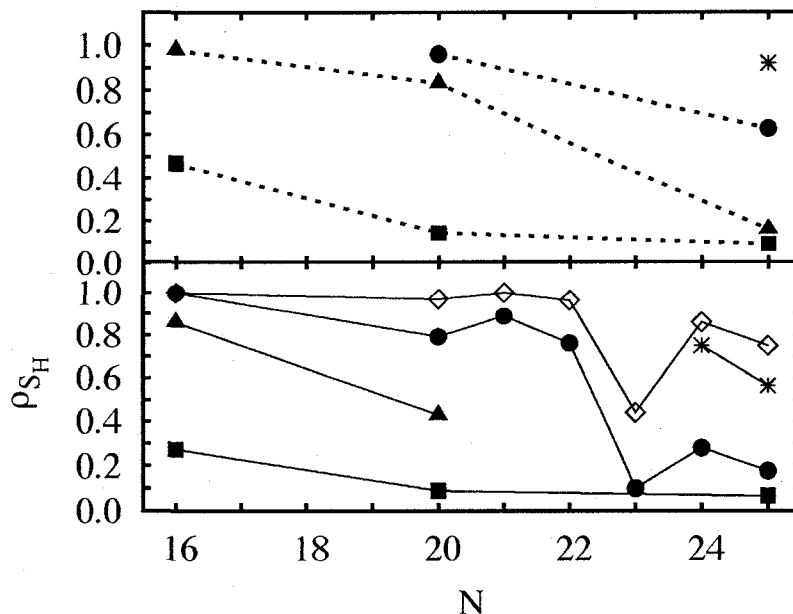


Figure 2.18: Superfluid fraction ρ_{SH} of the *para*-hydrogen component in clusters of N molecules with one (circles), two (triangles) and four (squares) substitutional *ortho*-deuterium molecules, and with one (stars) *ortho*-hydrogen molecule. Upper panel shows data at $T=0.5$ K, lower at $T=1$ K. Open diamonds show results for the undoped clusters (entirely superfluid at $T=0.5$ K). Error bars are comparable to the size of the symbols.

$(p\text{-H}_2)_{25}$ cluster causes ρ_{SH} to drop from 75% to less than 20% at $T=1$ K, while at $T=0.5$ K an almost complete suppression of the superfluid fraction is observed, in the same cluster, when two $p\text{-H}_2$ molecules are replaced by $o\text{-D}_2$. It should also be noted that pristine $p\text{-H}_2$ clusters with more than 22 molecules, generally display solid-like behavior even when undoped, albeit to different degrees [e.g., $(p\text{-H}_2)_{23}$ at $T=1$ K (see section 2.1)]

Fig. 2.19 compares the radial density profile (at $T=1$ K) of the (largely super-

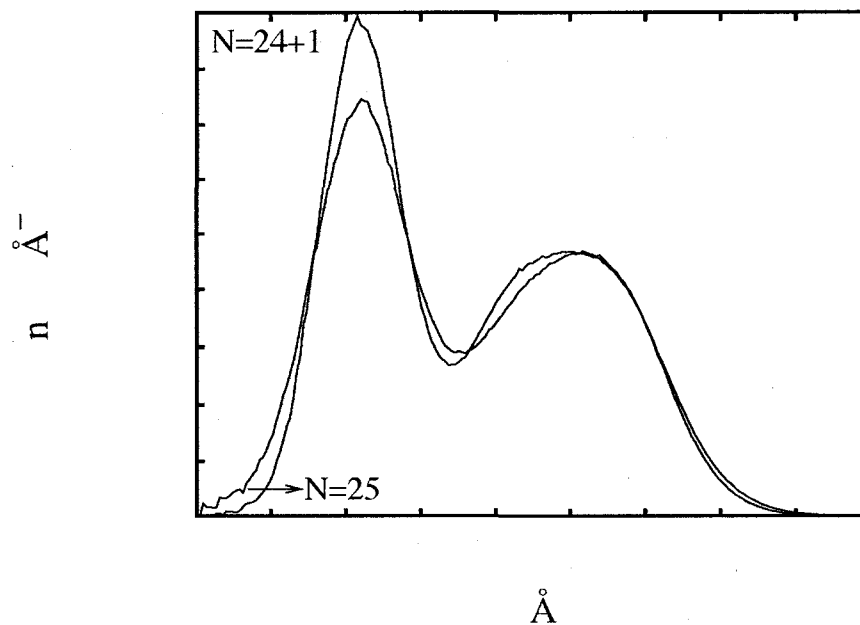


Figure 2.19: Radial density profiles for a pure $(p\text{-H}_2)_{25}$ (lower peak at short r) and a $(p\text{-H}_2)_{24}-(o\text{-D}_2)_1$ cluster, at $T=1$ K. Profiles are computed with respect to the geometrical center of the cluster. In the case of the doped cluster, no distinction is made between molecules of different types. Statistical errors are not shown for clarity; they are of the order of $5.0 \times 10^{-4} \text{ \AA}^{-3}$.

fluid) pristine $(p\text{-H}_2)_{25}$ cluster, with that of the (essentially insulating) cluster with the same number of molecules, but with one $p\text{-H}_2$ replaced by an $o\text{-D}_2$. Profiles are computed with respect to the geometrical center of the cluster (in the case of a mixed cluster, no distinction is made between molecules of different types). The main structural change arising from the substitution of a $p\text{-H}_2$ clearly occurs in the center of the cluster where molecules are more localized. In the vicinity of the surface of the system, density profiles are, in fact, almost identical.

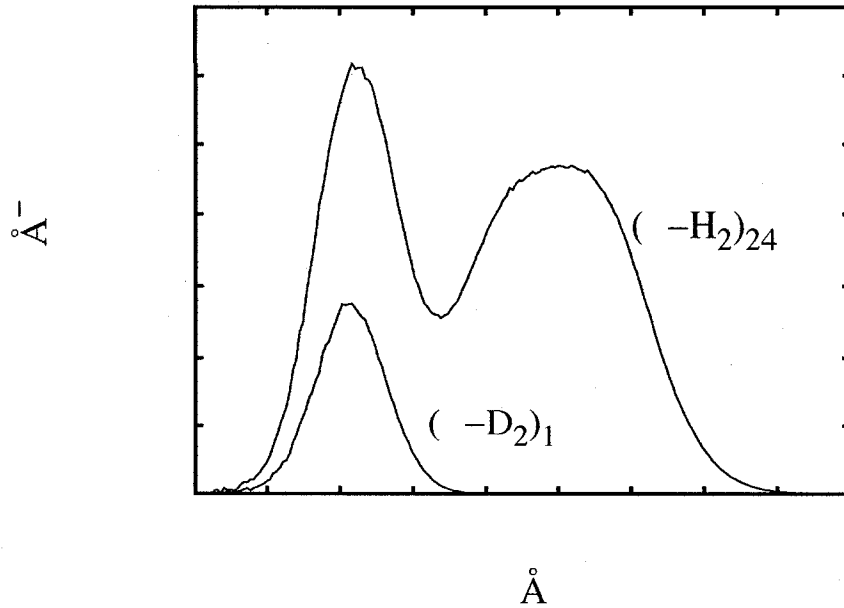


Figure 2.20: Radial density profiles of the two components of the cluster $(p-H_2)_{24}-(o-D_2)_1$ (at a temperature of 1 K) taken separately. Profiles are computed with respect to the geometrical center of the cluster.

If the dopant is $o-H_2$, on the other hand, then the structure of the cluster and its superfluid properties are much less sensitive to the substitution (see Fig. 2.18). For example, the corresponding profile for the cluster doped with one $o-H_2$ molecule is indistinguishable from that of the pristine cluster, on the scale of Fig. 2.19.

An important observation is that a lone $o-D_2$ molecule sits in the first shell of the cluster (see Fig. 2.20); this is something that we observe for all cluster studied here, with up to four $o-D_2$ substitutional impurities, in agreement with previous work [36]. The lighter $o-H_2$ dopant, conversely, is considerably more delocalized,

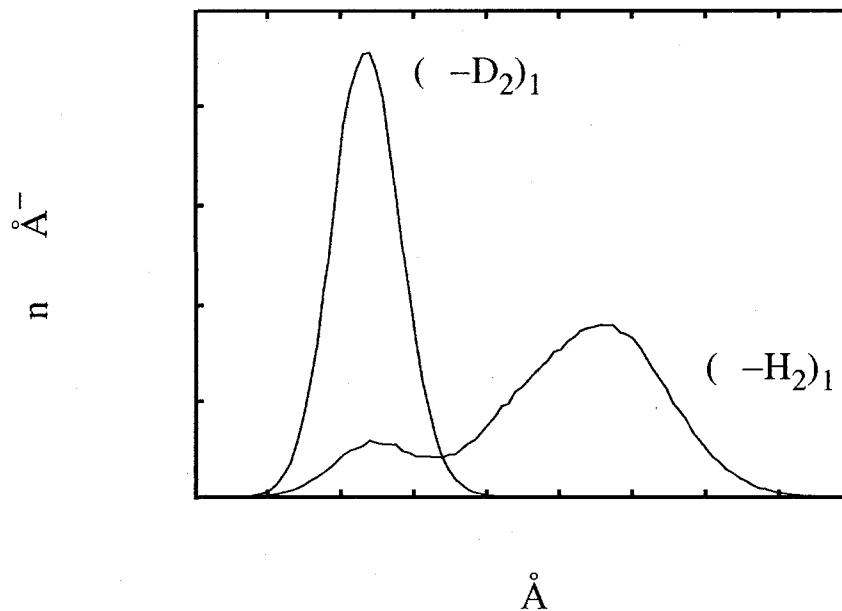


Figure 2.21: Radial density (multiplied by r^2) for the single o -D₂ and o -H₂ impurities in the doped $(p\text{-H}_2)_{24}-(o\text{-D}_2)_1$ and $(p\text{-H}_2)_{24}-(o\text{-H}_2)_1$ clusters, at a temperature of 1 K. Profiles are computed with respect to the geometrical center of the cluster.

and indeed is found prevalently in the external part of the cluster, as shown in Fig. 2.21.

The effect of cluster “crystallization,” induced in relatively large clusters by one or two o -D₂ impurities (and the ensuing suppression of p -H₂ SF) can also be observed in smaller systems, but a greater number of substitutions is needed. Fig 2.22 shows the structures of the two clusters $(p\text{-H}_2)_{16}-(o\text{-D}_2)_4$ (part A of the figure), and $(p\text{-H}_2)_{20}$ (part B); these pictures were obtained using the procedure outlined in Ref. [31]. The pristine cluster has a featureless structure, and is entirely

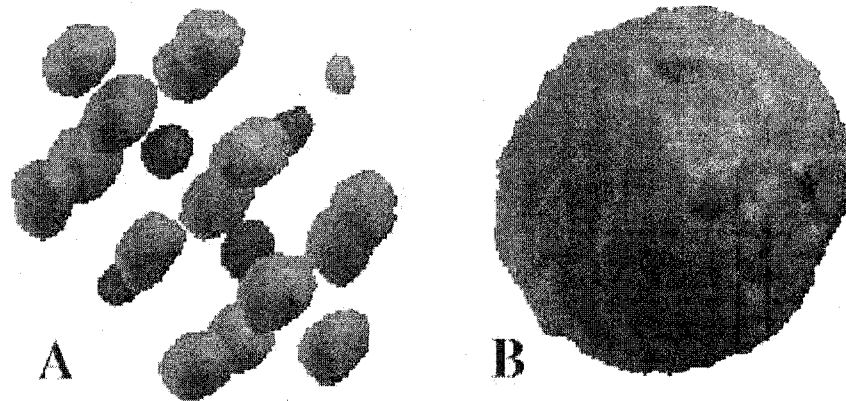


Figure 2.22: Three-dimensional representations of the clusters $(p\text{-H}_2)_{16}-(o\text{-D}_2)_4$ (A) and of $(p\text{-H}_2)_{20}$ (B). Darker color is used for impurity molecules.

superfluid at $T \leq 1$ K. On the other hand, ρ_{SF} is small in the doped cluster, whose solid-like structure is evident, with a central axis surrounded by rings of molecules. Two of the four $o\text{-D}_2$ molecules are placed on the axis, the other two on the central ring.

Numerical studies by other authors [31, 80] had already yielded evidence of localization of $p\text{-H}_2$ molecules around a heavy impurity, rendering small, pristine clusters [e.g., $(p\text{-H}_2)_{13}$] significantly more rigid and solid-like. In all previous works, however, impurities were considered such as CO, or HF, not only significantly heavier, but, more importantly, featuring a stronger (more attractive) interaction with the $p\text{-H}_2$ molecules, than that between the molecules themselves.

The results presented here, offer insight into the microscopic mechanism of SF in quantum clusters. In order for SF to occur, clusters (either doped or pristine) must be essentially liquid-like in character, i.e., molecules must enjoy a high degree of mobility and delocalization. The most important structural difference between

clusters that are insulating or superfluid at $T \leq 1$ K, also based on the results for pristine clusters discussed in sections 2.1 is that the former feature a rigid, solid-like core, possibly with some loosely bound molecules on the surface; on the other hand, SF is enhanced in clusters whose inner region is floppy, with exchanges taking place between molecules in the inner and outer shells.

This is consistent with the notion of *quantum melting* of large clusters, at low T (see section 2.1.3), originating from permutational exchanges involving *all* molecules, including those located in the inner part of the cluster. These exchanges become increasingly important at low temperature, where clusters become increasingly liquid-like, and consequently superfluid.

Fig. 2.23 displays the frequency with which exchange cycles of varying length (i.e., involving a different number $1 \leq M \leq N_H$ of $p\text{-H}_2$ molecules) occur (spikes from left to right) in a pristine $(p\text{-H}_2)_{25}$ cluster as well as in the mixtures $(p\text{-H}_2)_{24}-(o\text{-H}_2)_1$ and $(p\text{-H}_2)_{24}-(o\text{-D}_2)_1$ at $T=1$ K. All exchange cycles are clearly suppressed in the cluster doped with a single $o\text{-D}_2$, but the reduction is most dramatic for very long cycles. Conversely, when the cluster is doped with an $o\text{-H}_2$, exchanges (other than the very longest one) take place at almost the same frequency as in the pristine cluster.

Thus, a single substitutional $o\text{-D}_2$, which is located in the center of the cluster owing to its greater mass, has a strong inhibiting effect on long exchanges of $p\text{-H}_2$ molecules. As a result, the cluster turns solid-like, and SF is altogether suppressed. Conversely, a single $o\text{-H}_2$ dopant molecule can effectively get out of the way, thereby allowing for a greater occurrence of long exchanges, including those involving $p\text{-H}_2$ molecules in the inner and the outer shell of the cluster. As a result, the doped $(p\text{-H}_2)_{24}-(o\text{-H}_2)_1$ cluster remains largely liquid-like, with a value of ρ_{SH} close to

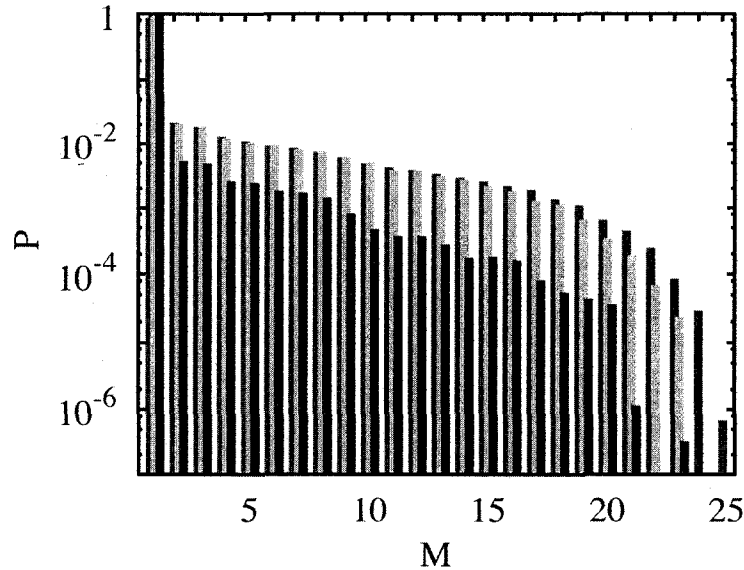


Figure 2.23: Frequency of occurrence of exchange cycles of length M (i.e., involving $1 \leq M \leq N_H$ p -H₂ molecules) at $T=1$ K. Spikes from left to right refer to a pristine $(p\text{-H}_2)_{25}$ cluster and to the mixtures $(p\text{-H}_2)_{24}-(o\text{-H}_2)_1$ and $(p\text{-H}_2)_{24}-(o\text{-D}_2)_1$.

60%.

The suggestion that SF is underlain, or strongly enhanced by the occurrence of exchange cycles involving also molecules located in the central region of the cluster is not in direct contradiction with the observation made in Ref. [42] that the superfluid density is largest at the surface. For, as discussed above the primary mechanism by which these exchanges promote SF is not by *locally* increasing the value of ρ_{SF} , but by stabilizing an overall liquid-like phase of the whole cluster. However, according to our results, the picture of SF, as arising from exchanges involving exclusively surface molecules, proposed in Ref. [42] seems not plausible.

2.4 50/50 Mixed clusters

Next we discuss mixed clusters with equal numbers of $p\text{-H}_2$ and $o\text{-D}_2$ molecules. The superfluid response of either component in these clusters, is generally not significant at a temperature as low as 0.5 K; In fact, as shown in Fig. 2.24, the average number $p\text{-H}_2$ or $o\text{-D}_2$ molecules in the superfluid phase do not exceed 2 for clusters comprising more than 10 molecules altogether (at $T=0.5$ K).

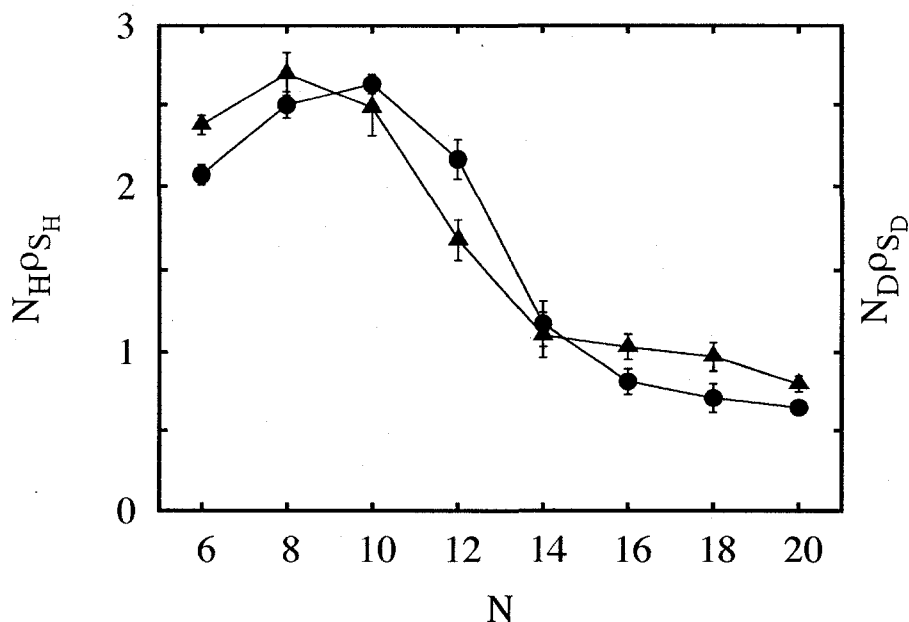


Figure 2.24: Number of $p\text{-H}_2$ (circles) and $o\text{-D}_2$ (triangles) molecules in the superfluid phase in mixed clusters of varying size N and equal concentration of the two isotopes (i.e., $N_H = N_D = N/2$) at $T=0.5$ K.

This suggests that at this temperature quantum effects are relatively modest in these systems, and therefore the mass difference is largely immaterial, the physical

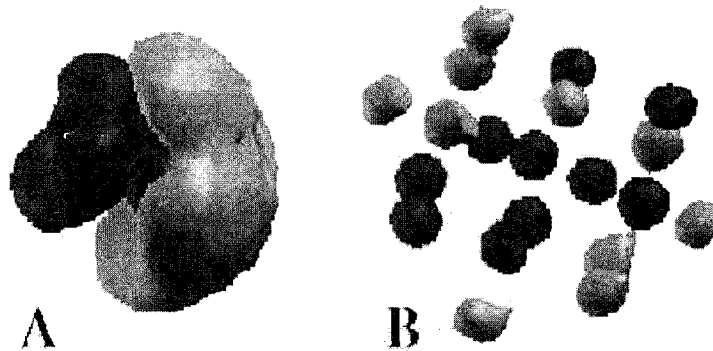


Figure 2.25: Three dimensional representation of the cluster $(p\text{-H}_2)_5\text{-(}o\text{-D}_2)_5$ (A) and $(p\text{-H}_2)_{10}\text{-(}o\text{-D}_2)_{10}$ (B) at a temperature of 0.5 K; $o\text{-D}_2$ molecules are rendered in darker color.

behavior being dominated by the potential energy.

It is notable that pristine clusters comprising $N=10$ $p\text{-H}_2$ or $o\text{-D}_2$ molecules, are superfluid at $T=0.5$ K, as shown in sections 2.1 and 2.2 while in the mixture $(p\text{-H}_2)_5\text{-(}o\text{-D}_2)_5$ SF is significantly suppressed. Therefore, the simultaneous presence of the two components mutually suppresses the superfluid response of both, and promotes a more solid-like arrangement of molecules.

Fig. 2.25 shows graphical representations of the three-dimensional structures of $(p\text{-H}_2)_5\text{-(}o\text{-D}_2)_5$ (part A) and $(p\text{-H}_2)_{10}\text{-(}o\text{-D}_2)_{10}$ (part B) clusters. While for the smaller cluster smearing of the molecules, attributed to zero-point motion, can be seen, the larger mixed cluster displays a classical structure, identical to that of a $(o\text{-D}_2)_{20}$ cluster³.

In the bulk, isotopic Bose mixtures are predicted theoretically to undergo spatial segregation at low temperature [81]. Our study shows that, even in clusters

³Simulations in progress for the mixed cluster $(p\text{-H}_2)_{10}\text{-(}o\text{-D}_2)_{10}$ at $T=0.0625$ K reveal incipient melting of the $o\text{-D}_2$ component which occupies the inner part of the system. This is consistent with the quantum melting observed in pure clusters, indicated by the ‘collapse’ of the first peak of the density profile (see Fig. 2.10).

of relative small size, such as the ones studied here, incipient de-mixing of the two species is easily recognizable, as already observed in classical binary LJ clusters [82, 83]. It should finally be noted that, while the increasing concentration of *o*-D₂ causes the entire cluster to turn progressively solid-like, isotopic separation is not observed to affect the structure in which the cluster crystallizes.

2.5 Local superfluidity of *p*-H₂ clusters

The results presented in section 2.3 suggest the connection between superfluid response and long permutational cycles of identical molecules throughout the whole system. One interesting open issue is how the superfluid response of a pure cluster is distributed across the droplet. Because a cluster is a finite non-homogeneous system, one may meaningfully pose the question of whether the decoupling from an externally applied rotation characterizing a superfluid is greater in some parts thereof (e.g., the surface). The relevance of this aspect goes obviously beyond the physics of *p*-H₂ clusters, as it impacts the general theoretical understanding of SF, and its connection with Bose condensation.

In a recent paper, Khairallah *et al.* utilized the radial density profile of particles involved in permutation cycles to study the local superfluid density of *p*-H₂ droplets. Based on their results, they concluded that the superfluid response is largely confined at surface of these small clusters, mainly arising from exchange cycles involving loosely bound surface molecules [42].

Aside from the difficulty of providing a meaningful definition of “surface” of clusters of such small size, the physical picture proposed in Ref. [42] is at odds with our results presented in the previous sections of this chapter for pure and

isotopically doped p -H₂ clusters, which have yielded, evidence that their superfluid response correlates with permutational exchange cycles comprising molecules in both the inner and the outer shell. Indeed, even clusters that display a coexistence of liquid- and solid-like behavior at $T \sim 1$ K [e.g., $(p\text{-H}_2)_{23}$] are essentially *entirely* superfluid in the liquid-like “phase” (see section 2.1.3), an observation which raises doubts about the contention that SF may be confined at the surface of the cluster.

In order to provide an independent theoretical check of the predictions of Ref. [42], we undertook a systematic study of the local superfluid properties of p -H₂ clusters at low temperature, using QMC simulations with a recently introduced, rigorous local superfluid density estimator [whose expression has been given in formula (1.37)], consistent with the basic two-fluid model [68].

Specifically we have computed the local superfluid density of pristine p -H₂ clusters of up to 27 molecules in the temperature range $0.0625 \text{ K} \leq T \leq 3 \text{ K}^4$, and examined its connection to global properties previously discussed in section 2.1.

Fig. 2.26 shows profiles of total $[n(r)]$ and superfluid $[n_S(r)]$ radial densities, computed with respect to the center of mass of the system, for a cluster comprising $N=18$ p -H₂ molecules. At $T=1$ K the cluster (see Fig. 2.3) is entirely superfluid, within the statistical uncertainty of our calculation. As shown in Fig. 2.26, the superfluid fraction is 100% everywhere in the cluster, with no sign of weakening near the center. At $T=2$ K, the total superfluid fraction of the cluster decreases to $\sim 55\%$; notably, however, the superfluid density remains finite throughout the cluster, even in its inner region. Upon increasing T to 3 K, the superfluid fraction drops to about 14% and $n_S(r)$ is correspondingly uniformly suppressed throughout the whole system, almost completely in correspondence of the total density

⁴Results presented in this section are obtained using the SG potential.

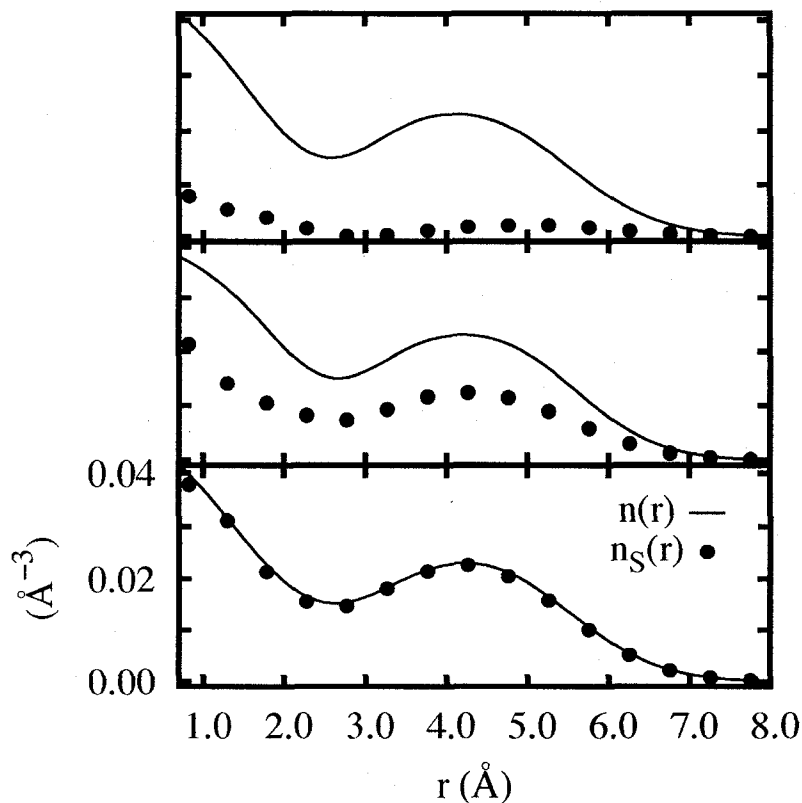


Figure 2.26: Profiles of total $[n(r)]$ and superfluid $[n_S(r)]$ density computed with respect to the center of mass of the cluster $(p\text{-H}_2)_{18}$ at $T=1$ K (lower panel), $T=2$ K (middle panel) and $T=3$ K (upper panel).

minimum. The latter information confirms the qualitative relation between SF and exchange cycles involving molecules in different spatial regions of the cluster. Clearly, the local superfluid response of this cluster is never confined to the surface. It is important to note that the discussed variations of $n_S(r)$ occur against a total density profile which is essentially unaffected by temperature, for this liquid-like cluster (as shown in Fig. 2.26).

A behavior analogous to that illustrated above for the $(p\text{-H}_2)_{18}$ cluster is dis-

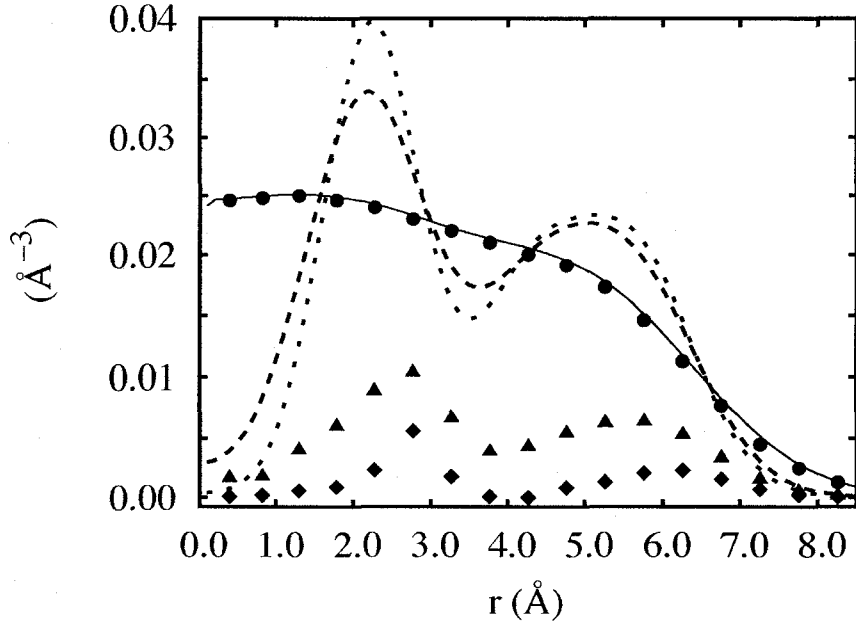


Figure 2.27: Profiles of total and superfluid density at $T=0.0625$ K (solid line and circles), $T=0.25$ K (dashed line and triangles) and $T=0.5$ K (dotted line and diamonds) for the cluster $(p\text{-H}_2)_{26}$.

played essentially by all clusters with fewer than 22 molecules, which are liquid-like in the temperature range considered here. As discussed in section 2.1, clusters with a number of molecules greater than 22 feature a different physical behavior, displaying (to different degrees) coexistence of liquid- and solid-like properties at $T \leq 1$ K. We discuss here the specific case $(p\text{-H}_2)_{26}$.

Fig. 2.27 shows the same profiles as Fig. 2.26 but for a cluster of $N=26$ molecules. This cluster displays insulating properties at $T=0.5$ K; its superfluid fraction is barely over 10%, rising to approximately 32% at $T=0.25$ K and reach-

ing 100% at $T=0.0625$ K. Correspondingly, and quite unlike the $N=18$ case, the structure of the cluster undergoes a significant change, as shown by the evolution of the radial density profile. In particular, the peak corresponding to the first shell (at $r \simeq 2$ Å) becomes suppressed as T decreases; hardly any remnant of the shell structure is left at $T=0.0625$ K, as a liquid-like structure emerges, i.e., the cluster undergoes quantum melting. Indeed, it is at low T (in contrast with what suggested in Ref. [42]), when this cluster quantum melts, that its basic physics becomes qualitatively reminiscent of that of a superfluid (liquid-like) helium cluster.

It is interesting to examine the corresponding evolution of the local superfluid density, also shown in Fig. 2.27. At the highest temperature shown, $n_S(r)$ is small at all distances from the center of mass, and negligible between the two shells (diamonds); here too it has to be stressed how, though the superfluid response is fractionally greater in the immediate surface (i.e., $r > 7$ Å), it is nonetheless not confined thereto. Moreover, as the temperature is lowered and the cluster turns liquid-like and superfluid, the relative increase of $n_S(r)$ is far more significant in its inner part. Especially telling is the disappearance of the dip in the region between the two shells (at $r \sim 4$ Å), suggesting the occurrence of permutations involving particles in both the inner and outer shell. This is consistent with the observed temperature dependence of the frequency of occurrence of permutation cycles involving different numbers of molecules, shown in Fig. 2.28.

We discussed in 2.1.2 the non-monotonic behavior of the total superfluid fraction of clusters of size $N \geq 22$; we further illustrate this phenomenon here, by focusing on a very narrow range of cluster sizes, within which the value of the superfluid fraction changes dramatically when adding just one molecule at a time. The results for the local superfluid, and total density definitively demonstrate that

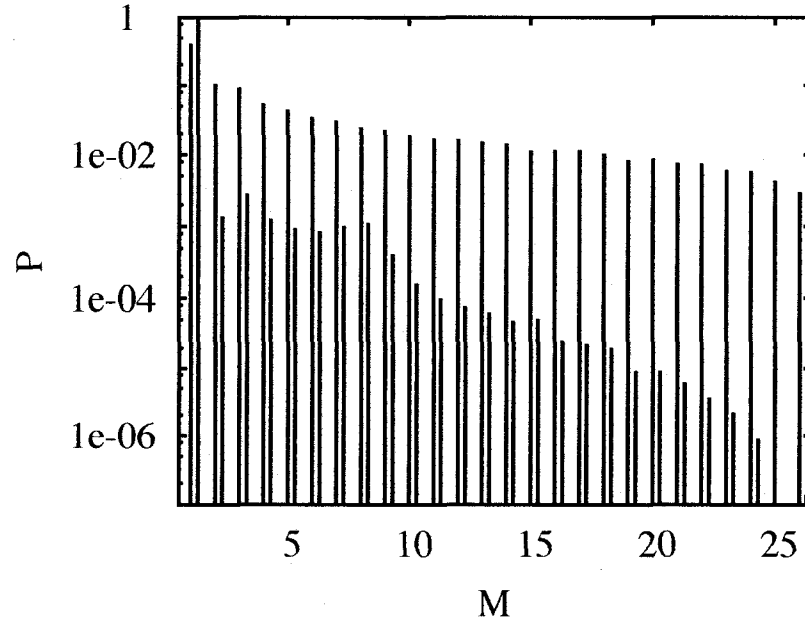


Figure 2.28: Frequency of occurrence of permutation cycles involving M molecules in a cluster of 26 p -H₂ molecules at $T=0.5$ K (lower values) and $T=0.0625$ K (higher values). Long permutation cycles set in at low T .

such behavior reflects structural changes throughout the *whole* cluster, not just its surface as contended in Ref. [42].

Total and superfluid densities for clusters of 25, 26 and 27 molecules at a temperature of 0.5 K are shown in Fig. 2.29. The superfluid fraction is close to 1 for $N=25$, dropping to roughly 0.12 for $N=26$ and rising again up to approximately 0.85 for $N=27$. For the $N=25$ cluster, the superfluid response is fractionally close to 100% throughout the entire cluster. While obviously fewer particles reside on average in the core than on the surface region of such a small cluster, the results

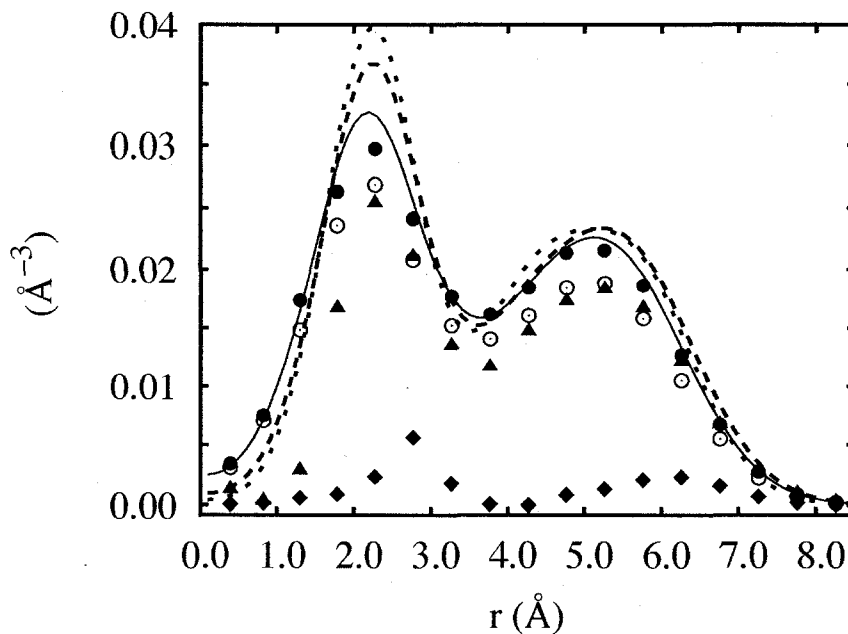


Figure 2.29: Profiles of total and superfluid density for the cluster $(p\text{-H}_2)_{25}$ (solid line and circles), $(p\text{-H}_2)_{26}$ (dotted line and diamonds), $(p\text{-H}_2)_{27}$ (dashed line and triangles) at $T=0.5$ K. Open symbols show estimates of the local superfluid density obtained for the cluster $(p\text{-H}_2)_{25}$ using the same measure utilized in Ref. [42].

of Fig. 2.29 again clearly show how SF is not confined to the surface, and the core of the cluster is not rigid but superfluid. The addition of a single molecule causes the entire cluster to turn abruptly insulating and solid-like, as shown by the increase in the height of the total density first shell peak. The local superfluid response is concurrently suppressed throughout the whole system, especially in the region between the two shells, to indicate the paucity of exchanges taking place between molecules in different shells. When adding yet another molecule, i.e., when increasing the cluster size to $N=27$, the cluster returns to a liquid-like structure,

and consistently the superfluid response is enhanced, at the surface, but also in the inner part of the system. These findings lend substantial theoretical support to the notion that the liquid-like, superfluid phase of these small clusters occurs as a result of the onset of long exchanges involving all molecules in the system. This is in fundamental disaccord with the picture put forth in Ref. [42], according to which SF would correlate to long exchanges involving loosely bound surface molecules.

One might be tempted to attribute the discrepancy of our results with those of Ref. [42] to the difference between the estimator of the local superfluid density utilized here, and the qualitative measure employed in Ref. [42], which lacks any microscopic justification [68, 23]. For comparison, we have performed a few calculations using that same measure, and found no substantial differences with our results (a comparison is shown in Fig. 2.29). Furthermore, our physical conclusions can also be inferred from the evolution of the density profiles as the temperature is lowered (Fig. 2.27), clearly showing the disappearance of the shell structure and the concurrent approach to unity of the *total* superfluid fraction (for this quantity the same estimator is used in our work and Ref. [42]), as well as by the temperature dependence of the frequency of occurrence of long permutation cycles (Fig. 2.28). All of this unambiguously shows that superfluidity correlates with long exchanges, comprising molecules both in the inner and outer shells.

More generally, it should be pointed out that the Continuous-space Worm Algorithm, utilized in this work, enjoys [37, 38] a much greater efficiency in sampling permutations than the method used in Ref. [42]. It is quite conceivable that the physical behavior observed in this work, underlain by long permutation cycles, may have remained hidden to the authors of Ref. [42], due to the inefficiency of

their method in sampling such cycles, especially at the lowest temperatures.

2.6 Dependence of the numerical estimates on the interaction potential

In this section, we examine in detail the dependence of our numerical results on the choice of the model interaction, pointing out how the physics described in this work does not depend on such a choice.

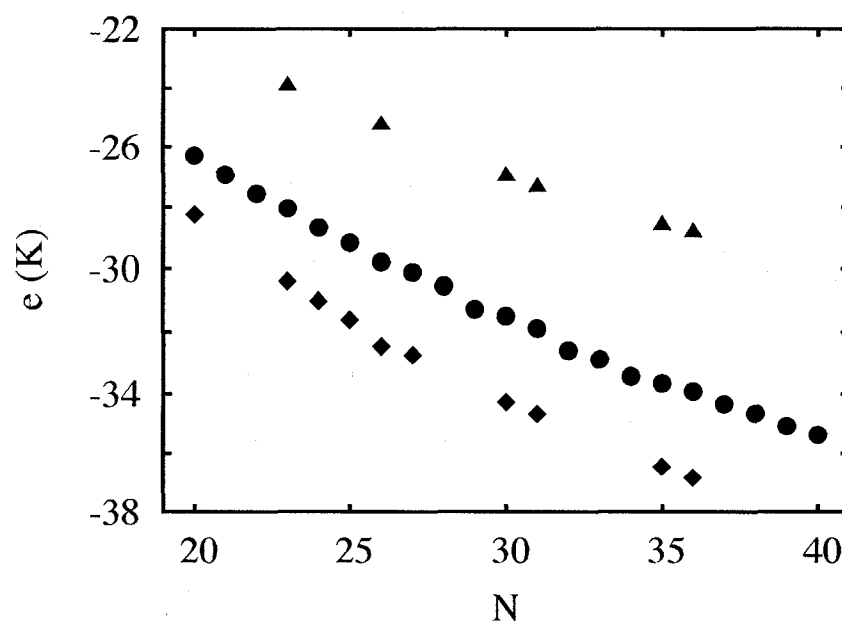


Figure 2.30: Energy per p -H₂ molecule as a function of the cluster size N at $T=1$ K. Estimates are obtained using the Buck (diamonds), SG (circles) and LJ (triangles) potential.

Although the SG potential (the one used in the majority of our calculations) is probably the best choice to describe the properties of molecular hydrogen (in small clusters as well as in the bulk) a comparison with other model interactions is due. Specifically, we compare estimates obtained with the SG, Buck, and LJ potential.

Fig. 2.30 shows the energy per p -H₂ molecule as a function of the cluster size N at a temperature of 1 K, computed with the LJ (triangles), Buck (diamonds) and SG (circles) potential. The values obtained with the Buck potential are ~ 2.5 K lower than those computed with the SG potential. This difference is consistent with the fact that the Buck potential is more attractive than the SG one. On the other hand, the energies estimated with the LJ potential display values up to 5 K higher than those calculated with the SG interaction. It seems therefore plausible that such a large quantitative difference may entail significantly different temperature dependence of some of the physical properties of interest.

Estimates of the superfluid fraction at $T=0.5$ K and $T=1$ K, as a function of the number of molecules in a p -H₂ cluster, are shown in Fig 2.31. Clusters of size up to ~ 20 molecules are largely superfluid at $T \leq 1$ K, and the computed values of ρ_S are essentially independent of the potential. When the cluster size increases, although a similar non monotonic trend of the superfluid fraction is observed regardless of the choice of the potential, important numerical discrepancies between results obtained with different potentials are evident. For example, a cluster comprising $N=26$ molecules at $T=0.5$ K is found to be insulating with the Buck or SG potential (open circles and diamonds), but 100% superfluid with the LJ one (open triangles). In general, the LJ potential yields a large superfluid response at a temperature considerably higher than that needed to detect the same superfluid response with

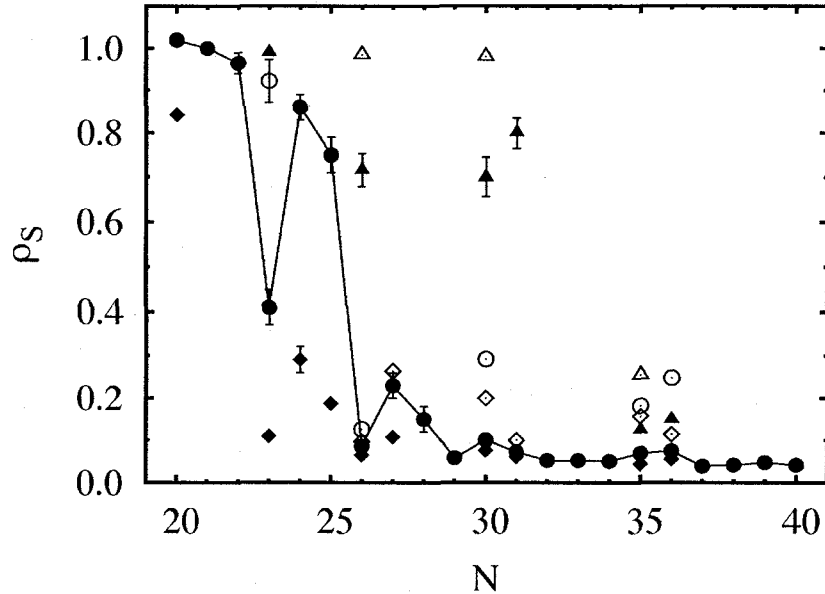


Figure 2.31: Superfluid fraction of p -H₂ clusters versus cluster size N at $T=1$ K (filled symbols) and $T=0.5$ K (open symbols). Estimates have been obtained using the SG (circles), Buck (diamonds) and LJ (triangles) potential.

the SG (or Buck) potential. However, it is crucial to stress that the physical mechanism by which clusters melt at low temperature, namely quantum melting, as well as all the other physical effects discussed in this work, are independent of the choice of the potential, whose only effect is to alter the energy scale.

Figures 2.32 and 2.33 illustrate the quantum melting phenomenon (extensively discussed in the case of the SG potential in section 2.1.3) when the LJ, or Buck, potential is used. In Fig. 2.32 we show the potential energy per particle (V) and the superfluid fraction of the cluster $(p\text{-H}_2)_{26}$ at $T=1$ K (panels a and b) and at $T=1.5$ K (panels c and d), computed in a typical Monte Carlo run. Estimates

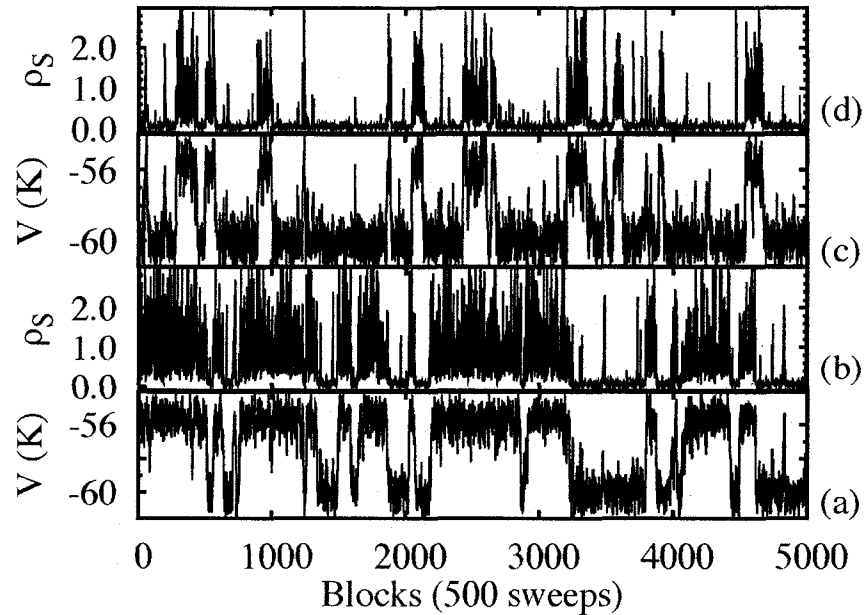


Figure 2.32: Potential energy per molecule and superfluid fraction observed during a typical Monte Carlo run for a cluster of $N=26$ p - H_2 molecules at $T=1$ K (panels a and b) and $T=1.5$ K (panels c and d). The coexistence of two phases can be easily recognized since the averages of ρ_S and V simultaneously switch between high (liquid-like superfluid phase) and low (solid-like insulating phase) values. The liquid-like superfluid phase becomes dominant as T is lowered. Results are obtained with the LJ potential.

are obtained with the LJ potential. The values of ρ_S and V (in analogy with the discussion offered in section 2.1.3 for a cluster of 23 p - H_2 molecules interacting via the SG potential) indicate the coexistence of a liquid-like (superfluid) and a solid-like (insulating) “phase”. The former becomes dominant at low T ; it is in fact at low T , that the cluster quantum melts.

Quantum melting occurs (at much lower T) even when the Buck potential is used. Fig. 2.33 shows profiles of radial density of $(p\text{-}H_2)_{26}$ at $T=1$ K and

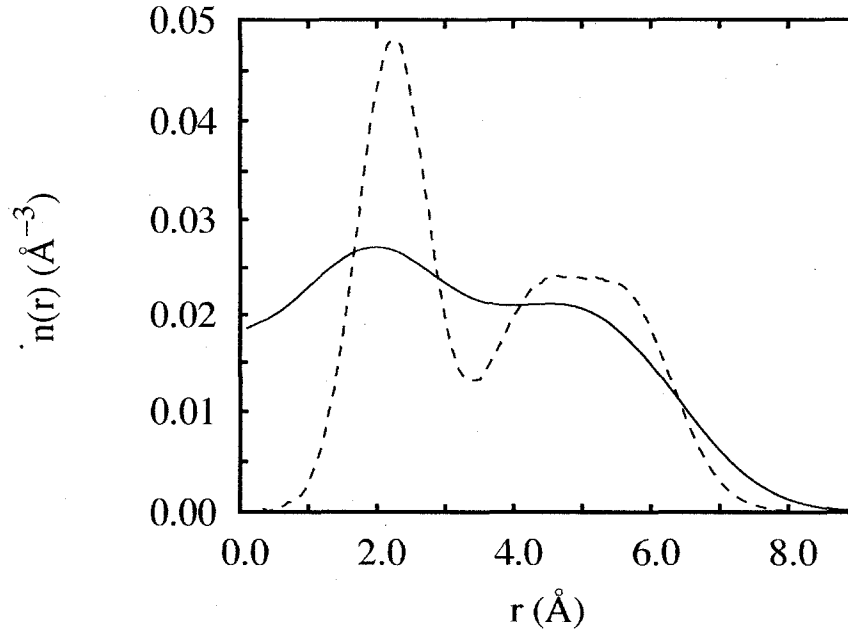


Figure 2.33: Radial density profiles for a p -H₂ cluster with $N=26$ at $T=0.0625$ K (solid line) and $T=1$ K (dashed line). The system undergoes quantum melting at low T . Statistical errors, not shown for clarity, are of the order of $5 \times 10^{-4} \text{ \AA}^{-3}$ or less, results are obtained with the Buck potential.

$T=0.0625$ K obtained with the Buck potential. At $T=1$ K the superfluid fraction (estimated with the Buck potential) of this cluster is approximately 0.06 and its structure is solid-like as indicated by the height of the first peak and by the pronounced inter-shell minimum of the density profile (dashed line). When T is lowered to 0.0625 K the value of ρ_S approaches 0.95 and concomitantly the cluster quantum melts becoming liquid-like and almost completely structureless as signaled by the “collapse” of the first-shell peak and by the persistent tail of density at long distances (solid line). Once again we stress that Fig. 2.32 and 2.33 show the

same physical phenomenon (i.e., the quantum melting) that occurs independently of the interaction potential employed.

CONCLUSIONS

We have presented results obtained by means of accurate Path Integral Monte Carlo simulations based on the Continuous-space Worm Algorithm for the low temperature ($0.0625 \text{ K} \leq T \leq 4 \text{ K}$) properties of pristine and isotopically doped hydrogen clusters of size up to $N=48$ molecules.

Pristine ($p\text{-H}_2$) $_N$ clusters comprising up to $N=21$ molecules are liquid-like and superfluid with a superfluid fraction $\rho_S \simeq 1$ at $T \leq 1 \text{ K}$. The superfluid fraction, for $N \geq 22$, displays a remarkable size dependence reflecting structural changes that occur on adding or removing even a single molecule. Coexistence of liquid-like (superfluid) and solid-like (insulating) phases has been shown in some clusters; the dominance of the former at low T indicates that these systems melt as a result of zero-point motion and quantum exchanges, freezing instead at high T . We refer to this intriguing behavior as *quantum melting*. Significant superfluid response has also been found, at $T=0.5 \text{ K}$, in $o\text{-D}_2$ clusters of size up to $N \sim 14$. The heavier mass of the $o\text{-D}_2$ molecules is responsible for the suppression of ρ_S in larger clusters. Some clusters, featuring specific numbers of particles, are characterized by greater stability; the fact that the “magic number” $N=13$ is present for both $p\text{-H}_2$ and $o\text{-D}_2$ clusters, suggests that its stability is associated with high symmetry, i.e., it is related to the potential energy. These structures, however, need not necessarily

be solid-like, but rather simply have filled coordination shells.

We have also studied mixed isotopically doped p -H₂ clusters of various sizes, down to $T=0.5$ K. To our knowledge, this is the first study of a mixed isotopic bosonic cluster including all quantum-mechanical effects, namely zero-point motion and permutations of identical particles. We find that the superfluid fraction of pure p -H₂ clusters is suppressed by replacement of few p -H₂ by o -D₂ molecules. The suppression is most dramatic for clusters with more than 22 molecules, which display (at $T \simeq 1$ K) incipient solid-like behavior even when pristine. The reduction of the superfluid fraction is considerably smaller in the presence of substitutional o -H₂ impurities. Lighter impurities, which are delocalized throughout the system, have less disruptive an effect on long exchanges than the heavier impurities, which sit in the inner part of the cluster. These findings are consistent with the notion of melting of pure clusters at low temperature as arising from purely quantum-mechanical effects, namely long exchanges of indistinguishable particles.

Mixed (50/50) (p -H₂)-(o -D₂) clusters comprising up to 20 molecules altogether are generally found to be non-superfluid at $T \simeq 0.5$ K. The fact that at this temperature the superfluid response is suppressed also in small ($N \sim 10$) mixed cluster is in contrast with what observed for pure p -H₂ (o -D₂) clusters of the same size which display pronounced superfluid response. The isotopic composition of mixed clusters, therefore, has the effect of suppressing the superfluid response of both components. Moreover we observed, even in small 50/50 mixtures, such as those studied in this work, incipient de-mixing of the two components.

The spatial distribution of superfluidity has been studied in pure p -H₂ clusters. We found no evidence of superfluid response confined at the surface, regardless of temperature and system size explored. Superfluidity concomitantly grows as

T decreases in the inner and outer part of the system in liquid-like clusters [i.e., $(p\text{-H}_2)_{18}$] as well as in those which feature quantum melting at low T . In the latter case, structural variations such as the progressive collapse of the first peak of the radial density profile are due to long (i.e., inter-shell) exchanges, involving all molecules in the cluster. Long exchanges cause the system to turn liquid-like at sufficiently low T , with the ensuing onset of superfluidity. Significant superfluid response is only seen when the core and the surface are both superfluid and liquid-like, i.e., it is not the effect of quantum exchanges involving exclusively, or mostly, surface molecules. These findings obtained by means of a rigorously defined estimator for the local superfluid density are at variance with recent calculations [42], performed by means of conventional Path Integral Monte Carlo, on the basis of a semi-empirical defined estimator. The main reason of this disagreement, however, seems related neither to the particular choice of the estimator nor to the different interaction potential utilized in Ref. [42]. Rather it might depend on the scarcely efficient sampling of many-particle permutations which affect the conventional Path Integral Monte Carlo approach.

We have carefully checked our physical conclusions and numerical estimates repeating most of the simulations with the Buck and Lennard-Jones potential. These model interactions have been shown to be somewhat less accurate than the Silvera-Goldman one, employed in the majority of our calculations and in most of the theoretical investigations of this kind, however they can provide an important benchmark for the relevant physical effects discussed in this work. Despite noticeable numerical discrepancies, due to the particular potential utilized, in the estimates of energetics and superfluid fraction, we observed quantum melting at low temperature driven by the onset of long quantum exchanges with all the three

interactions. For example a p -H₂ cluster of 26 molecules interacting via the Silvera-Goldman potential is almost completely molten at $T=0.125$ K, at half of this value in the case of the Buck interaction and at T of the order of 1 K when the Lennard-Jones interaction is used. Evidence is therefore found that the mechanism by which clusters melt at low T is independent of the specific interaction potential whose unique effect is to alter the energy and temperatures scale.

The study of Bose-Einstein condensation in small clusters appears to be the natural extension of this work. In particular estimates of "condensate" density profiles (obtainable by the one-body density matrix) can be used together with the information given by profiles of superfluid density to gain additional insight into the relation, still not well established, between superfluidity and Bose-Einstein condensation. Moreover simulations in progress on large 50/50 (p -H₂)-(o -D₂) mixed clusters at $T=0.0625$ K, revealing the incipient melting of the inner part of the cluster, occupied by the heavier component, encourage us to explore lower temperature regimes with the reasonable expectation of finding an example of superfluid bosonic mixture.

Bibliography

- [1] D. R. Tilley and J. Tilley. *Superfluidity and Superconductivity*. John Wiley and Sons Inc, New York, 1974.
- [2] L. Kapitsa. *Nature*, 141:74, 1938.
- [3] J. F. Allen and A. D. Misener. *Nature*, 141:75, 1938.
- [4] W. H. Keesom and G. E. MacWood. *Physica*, 5:737, 1938.
- [5] L. Tisza. *Nature*, 141:913, 1938.
- [6] E. L. Andronikashvili. *J. Phys. U. S. S. R.*, 10:201, 1946.
- [7] F. Dalfovo, S. Giorgini, L. P. Pitaevsky, and S. Stringari. *Rev. Mod. Phys.*, 71:463, 1999.
- [8] V. L. Ginzburg and A. A. Sobyenin. *JETP Lett.*, 15:1972, 1972.
- [9] The fascinating suggestion that a *crystal* may flow without dissipation has been the subject of much recent interest (E. Kim and M. H. W. Chan. *Nature*, 427:225, 2004). Still, it is commonly accepted that SF ought to be more easily observed in liquids.
- [10] M. Bretz and A. L. Thomson. *Phys. Rev. B*, 24:467, 1981.

- [11] G. M. Seidel, H. J. Maris, F. I. B. Williams, and J. G. Cardon. *Phys. Rev. Lett.*, 56:2380, 1986.
- [12] G. M. Seidel, H. J. Maris, and F. I. B. Williams. *Phys. Rev. B*, 36:6799, 1987.
- [13] M. Schindler, A. Dertinger, Y. Kondo, and F. Pobell. *Phys. Rev. B*, 53:11451, 1996.
- [14] M. Wagner and D. M. Ceperley. *J. Low Temp. Phys.*, 102:275, 1996.
- [15] K. Nho and E. Manousakis. *Phys. Rev. B*, 65:115409, 2002.
- [16] M. Boninsegni. *Phys. Rev. B*, 70:125405, 2004.
- [17] M. Boninsegni. *Phys. Rev. B*, 70:193411, 2004.
- [18] M. C. Gordillo and D. M. Ceperley. *Phys. Rev. Lett.*, 79:3010, 1997.
- [19] M. Boninsegni. *New J. Phys.*, 7:78, 2005.
- [20] S. Goyal, D. L. Schutt, and G. Scoles. *Phys. Rev. Lett.*, 69:933, 1992.
- [21] A. F. Vilesov, J. P. Toennies, and K. B. Whaley. *Physics Today*, 54, 2001.
- [22] S. Grebenev, B. Sartakov, J. P. Toennies, and A. F. Vilesov. *Science*, 289:1532, 2000.
- [23] E. W. Draeger and D. M. Ceperley. *Phys. Rev. Lett.*, 90:065301, 2003.
- [24] S. Moroni, A. Sarsa, S. Fantoni, K. Schmidt, and S. Baroni. *Phys. Rev. Lett.*, 90:143401, 2003.
- [25] J. Tang, A. R. McKellar, F. Mezzacapo, and S. Moroni. *Phys. Rev. Lett.*, 92:145503, 2004.

- [26] F. Mezzacapo. *J. Low. Temp. Phys.*, 140:241, 2005.
- [27] S. Moroni, N. Blinov, and P. N. Roy. *J. Chem. Phys.*, 121:3577, 2004.
- [28] Y. Kwon and K. B. Whaley. *Phys. Rev. Lett.*, 89:273401, 2002.
- [29] F. Paesani, R. E. Zillich, and K. B. Whaley. *J. Chem. Phys.*, 122:181106, 2005.
- [30] Y. Kwon and K. B. Whaley. *J. Low. Temp. Phys.*, 140:227, 2005.
- [31] S. Baroni and S. Moroni. *ChemPhysChem*, 6:1884, 2005.
- [32] S. Moroni, M. Botti, S. de Palo, and A. R. McKellar. *J. Chem. Phys.*, 122:0943114, 2005.
- [33] M. Zoppi. *J. Phys. CM*, 15:1047, 2003.
- [34] G. Tejada, J. M. Fernandez, S. Montero, D. Blume, and J. P. Toennies. *Phys. Rev. Lett.*, 92:223401, 2004.
- [35] P. Sindzingre, D. M. Ceperley, and M. L. Klein. *Phys. Rev. Lett.*, 67:1871, 1991.
- [36] C. Chakravarty. *Phys. Rev. Lett.*, 75:1727, 1995.
- [37] M. Boninsegni, N. Prokof'ev, and B. V. Svistunov. *Phys. Rev. Lett.*, 96:070601, 2006.
- [38] M. Boninsegni, N. Prokof'ev, and B. V. Svistunov. *Phys. Rev. E*, 74:036701, 2006.
- [39] D. M. Ceperley. *Rev. Mod. Phys.*, 67:279, 1995.

- [40] F. Mezzacapo and M. Boninsegni. *Phys. Rev. Lett.*, 97:045301, 2006.
- [41] F. Mezzacapo and M. Boninsegni. *Phys. Rev. A*, 75:033201, 2007.
- [42] S. A. Khairallah, M. B. Sevryuk, D. M. Ceperley, and J. P. Toennies. *Phys. Rev. Lett.*, 98:13401, 2007.
- [43] F. Mezzacapo and M. Boninsegni. *Phys. Rev. Lett.*, 100:145301, 2008.
- [44] F. Mezzacapo and M. Boninsegni. *Phys. Rev. A*, 76:021201, 2007.
- [45] I. F. Silvera and V. V. Goldman. *J. Chem. Phys.*, 69:4209, 1978.
- [46] U. Buck, F. Huisken, A. Kohlhase, D. Otten, and J. Schaeffer. *J. Chem. Phys.*, 78:4439, 1983.
- [47] F. Mezzacapo and M. Boninsegni. In preparation.
- [48] B. L. Hammond, W. A. Lester, and P. J. Reynolds. *Monte Carlo Methods in Ab Initio Quantum Chemistry*. World Scientific, Singapore, 1994.
- [49] S. Moroni and S. Baroni. *Phys. Rev. Lett.*, 82:4745, 1999.
- [50] J. E. Cuervo and P. N. Roy. *J. Chem. Phys.*, 125:124314, 2006.
- [51] R. Guardiola and J. Navarro. *Phys. Rev. A*, 74:025201, 2006.
- [52] R. Guardiola and J. Navarro. *Cent. Eur. J. Phys.*, 6:33, 2008.
- [53] H. Jiang and Z. Bacic. *J. Chem. Phys.*, 122:244306, 2005.
- [54] F. Operetto and F. Pederiva. *J. Chem Phys.*, 126:074704, 2007.
- [55] F. Operetto and F. Pederiva. *Phys. Rev. B*, 73:184124, 2006.

- [56] R. P. Feynman. *Rev. Mod. Phys.*, 20:348, 1948.
- [57] W. H. Press, S. A. Teukolsky, W. T. Vetterling, and B. P. Flannery. *Numerical Recipes: the Art of Scientific Computing*, chapter 7. Cambridge University Press, 1992.
- [58] N. Metropolis, A. Rosenbluth, M. N. Rosenbluth, A. H. Teller, and E. Teller. *J. Chem. Phys.*, 21:1087, 1953.
- [59] D. M. Ceperley and E. L. Pollock. *Phys. Rev. Lett.*, 56:351, 1986.
- [60] M. Boninsegni, N. V. Prokof'ev, and B. V. Svistunov. *Phys. Rev. Lett.*, 96:105301, 2006.
- [61] L. Pollet, M. Boninsegni, A. B. Kuklov, N. V. Prokof'ev, B. V. Svistunov, and M. Troyer. *Phys. Rev. Lett.*, 99:035301, 2007.
- [62] M. Boninsegni, A. B. Kuklov, L. Pollet, N. V. Prokof'ev, B. V. Svistunov, and M. Troyer. *Phys. Rev. Lett.*, 97:080401, 2006.
- [63] M. Boninsegni, A. B. Kuklov, L. Pollet, N. V. Prokof'ev, B. V. Svistunov, and M. Troyer. *Phys. Rev. Lett.*, 98:135301, 2007.
- [64] J. E. Cuervo, P. N. Roy, and M. Boninsegni. *J. Chem. Phys.*, 122:114504, 2005.
- [65] S. Jang, S. Jang, and G. A. Voth. *J. Chem. Phys.*, 115:7832, 2001.
- [66] P. Sindzingre, M. L. Klein, and D. M. Ceperley. *Phys. Rev. Lett.*, 63:1601, 1989.
- [67] Y. Kwon and K. B. Whaley. *Phys. Rev. Lett.*, 83:4108, 1999.

- [68] Y. Kwon, F. Paesani, and K. B. Whaley. *Phys. Rev. B*, 74:174522, 2006.
- [69] H. Flyvbjerg and H. G. Petersen. *J. Chem. Phys.*, 91:461, 1989.
- [70] O. Kornilov, J. Navarro, and J. P. Toennies. *J. Chem. Phys.*, 124:084307, 2006.
- [71] D. Blume. Private communication.
- [72] G. G. Batrouni and R. T. Scalettar. *Phys. Rev. Lett.*, 84:1599, 2000.
- [73] D. Scharf, M. L. Klein, and G. J. Martyna. *J. Chem. Phys.*, 97:3590, 1992.
- [74] R. E. Kunz and R. S. Berry. *Phys. Rev. Lett.*, 71:3987, 1993.
- [75] C. Predescu, P. A. Frantsuzov, and V. A. Mandelshtam. *J. Chem. Phys.*, 122:154305, 2005.
- [76] F. Calvo, J. P. K. Doye, and D. J. Wales. *J. Chem. Phys.*, 114:7312, 2001.
- [77] C. Predescu, D. Sabo, and J. D. Doll. *J. Chem. Phys.*, 119:12119, 2001.
- [78] *ortho*-deuterium naturally occurs as a mixture of $S=0$ and $S=2$ spin states.
- [79] J. E. Cuervo. Private communication.
- [80] F. Sebastianelli, Y. S. Elmatad, H. Jiang, and Z. Bacic. *J. Chem. Phys.*, 125:164313, 2006.
- [81] M. D. Miller. *Phys. Rev. B*, 18:4730, 1978.
- [82] A. S. Clarke, R. Kapral, B. Moore, G. Patey, and X. G. Wu. *Phys. Rev. Lett.*, 70:3823, 1993.
- [83] A. S. Clarke, R. Kapral, and G. Patey. *J. Chem. Phys.*, 101:2432, 1994.